Dynamic Undocking and the Quasi-Bound State as Tools for Drug Design

Sergio Ruiz-Carmona,[1] Peter Schmidtke,[2] F. Javier Luque,[1] Lisa Baker,[3] Natalia Matassova,[3] Ben Davis,[3] Stephen Roughley,[3] James Murray,[3] Rod Hubbard,[3,4] Xavier Barril[1,5,*]

[1] Institut de Biomedicina de la Universitat de Barcelona (IBUB) and Facultat de Farmàcia, Universitat de Barcelona, Av. Joan XXIII s/n, 08028 Barcelona, Spain.

[2] Discngine, 33 rue du Fauburg Saint-Antoine, 75011 Paris, France

[3] Vernalis (R&D) Ltd, Granta Park, Cambridge, CB21 6GB, UK

[4] YSBL, University of York, Heslington, York, YO10 5DD, UK

[5] Catalan Institution for Research and Advanced Studies (ICREA), Passeig Lluís Companys 23, 08010 Barcelona, Spain.

* Send correspondence to: xbarril@ub.edu

There is a pressing need for new technologies that improve the efficacy and efficiency of drug discovery. Structure-based methods have contributed towards this goal but they focus on predicting the binding affinity of protein–ligand complexes, which is notoriously difficult. We adopt an alternative approach that evaluates structural, rather than thermodynamic, stability. Noting that bioactive molecules present a static binding mode, we devised Dynamic Undocking (DUck), a fast computational method to calculate the work necessary to reach a quasi-bound state, where the ligand has just broken the most important native contact with the receptor. This non-equilibrium property is surprisingly effective in virtual screening because true ligands form more resilient interactions than decoys. Notably, DUck is orthogonal to docking and other 'thermodynamic' methods. We demonstrate the potential of the docking–undocking combination in a fragment screening against the molecular chaperone and oncology target Hsp90, for which we obtain novel chemotypes and a hit rate approaching 40%.

Structural stability is a fundamental property of protein–ligand complexes. Though cases of dual binding modes have been reported,[1,2] they are generally not dynamic, or involve predominantly hydrophobic interactions,[3] which lack directionality and do not impose strict geometric constraints.[4] By contrast, hydrogen bonds are ideal to provide structural stability because they have sharp distance and angular dependencies.[4] Their contribution to the free energy of binding (ΔG_{bind}) is variable but can be substantial.[5] Importantly, they often act as anchoring points in protein–ligand complexes, providing the minimal binding unit through one or a few hydrogen bonds as demonstrated for fragment-sized ligands.[6,7] We have previously shown that certain hydrogen bonds present strong opposition to small structural distortions and can act as kinetic traps because the local environment hinders the transition from a direct hydrogen bond to a water-bridged interaction.[8] As an early unbinding event, rupture of the so-called water-shielded hydrogen bonds can influence the whole dissociation process.[8,9] Taken together, these observations suggest that hydrogen bonds are the main determinants of structural stability, and lead us to postulate that their resilience should provide information about the binding potential of candidate ligands. Thus, we set out to investigate whether the work required to disrupt intermolecular hydrogen bonds can be used to predict ligand binding.

We will introduce DUck, a simplified computational procedure to calculate the work needed to break a key native contact, reaching a quasi-bound state (W_{QB}). Then, we will show that active compounds are structurally stable and present higher W_{QB} values than inactive ones. Finally, we demonstrate the use of this

property in virtual screening (VS) applications, showing that DUck complements the thermodynamic perspective offered by existing methods.

Results and Discussion

Simplified simulation of the early dissociation stage

To assess the hypothesis, we have devised Dynamic Undocking (DUck) simulations, where a key intermolecular hydrogen bond is pulled from an initial distance of 2.5 Å (close contact) to 5.0 Å (broken contact). In order to focus on just one specific hydrogen bond, we use model receptors comprising only the protein residues that are within 6 Å of the given hydrogen bond (Figure 1A). The work necessary to carry out the steering process is monitored, and we define the quasi-bound (QB) state as the point along the simulation where the work profile presents the highest value. W_{QB} is the work necessary to depart from the ideal hydrogen bond configuration and reach the QB state (Figure 1B). Notably, this is a non-equilibrium property, and there is no reason why it should correlate with any measurement of binding affinity. What is more, as the unbound state is not considered, W_{QB} cannot inform about the binding free energy. Instead, this magnitude solely indicates if the interaction under investigation gives rise to a (local) minimum in the free energy landscape and estimates the depth of said minimum (Supplementary Figure 1).

Relationship between W_{QB} and binding affinity

As an initial proof of concept, we apply DUck to a set of 41 fragment-like ligands (<300Da) of the cyclin dependent kinase 2 (CDK2) with known binding mode and half maximal inhibitory concentration (IC_{50}) values. The hinge region of all kinases is a hot spot for binding, where the protein backbone offers privileged hydrogen-bonding opportunities.[10] For CDK2, the central hydrogen-bond donor (NH of Leu83) is the most conserved interaction site and was used to define the reaction coordinate. W_{QB} presents only a weak correlation with binding affinity (Supplementary Figure 2), but the distribution of W_{QB} values is clearly skewed (Figure 2A and Supplementary Figure 3). Thus, 65% of weak binders (IC_{50} > 1 μM) present W_{QB} values below 6 kcal/mol, while all strong binders (IC_{50} < 1 μM) pass this threshold. Ligand 3FZ1,[11] is the clear exception as it presents an almost flat dissociation profile (W_{QB} = 0.12 kcal/mol). This is explained by an unsuitably long (3.4 Å) interaction with the hinge region, involving a methoxy group, which is a poor hydrogen bond acceptor.[4] Instead, this unusual ligand forms two charge-reinforced hydrogen bonds with Lys33 and Asn132, from which it draws structural stability (Supplementary Figure 4). This shows that some ligands can use alternative or additional interaction points to attain structural stability, in which case, DUck calculations (as currently implemented) may underestimate the cost of breaking the native contacts.

To further examine the surprising relationship between binding affinity and W_{QB}, we use the bromodomain and extra-terminal (BET) BRD4-BD1 as additional test system. The side-chain N of Asn140 is a well-known pharmacophoric point of this epigenetic target,[12] and defines the key intermolecular hydrogen bond. Again, we observe the same trend, i.e. higher W_{QB} for more potent ligands, but with a large

dispersion that blurs correlation (Supplementary Figures 3 and 5). Interestingly, the lowest W_{QB} values (0, 1.1 and 1.7 kcal/mol) correspond to three kinase inhibitors with off-target activity for the BRD4-BD1.[13] Thus, achieving potency in the absence of a robust anchoring interaction is possible, but rare, which suggests that it is an ineffective strategy.

DUck is very effective in virtual screening

We then assess whether the approach can be used in virtual ligand screening by testing the ability of DUck to distinguish true CDK2 ligands from a set of carefully selected decoys[14] for which we had generated binding modes by docking. The distribution of W_{QB} is strikingly different from the active set, with 61% of molecules presenting values below 2 kcal/mol and 49% below 1 kcal/mol (Figure 2A). This indicates that, in spite of forming the key hydrogen bond, this interaction is labile for most of the docking decoys, which would translate to an unstable binding mode. We therefore propose that W_{QB} can distinguish true ligands from inactive molecules, as shown in the receiver operating characteristics (ROC) curves (Figure 2B). To demonstrate the wider applicability of the method, we conducted similar experiments with the adenosine A2A receptor (AA2R) and Trypsin, as representatives of G protein-coupled receptors (GPCR) and serine proteases, respectively (Figure 2B). Together with kinases (such as CDK2) these protein families include a large part of the current and investigational drug targets.[15] The key hydrogen bonds tracked by the DUck simulations involve the side-chain carbonyl of Asn253, in the case of AA2R, and the carboxylic acid of Asp189, for Trypsin. As shown in Figure 2B, the results for these systems are even better than for CDK2, demonstrating that DUck is surprisingly effective in virtual screening.

Importantly, the performance improves consistently as sampling increases, but good enrichments can be obtained with as little as 2 DUck runs per ligand (Supplementary Figure 6).

DUck is orthogonal to existing methods

These results position DUck as a new method for virtual screening. But, as it aims to predict a property that is fundamentally different from thermodynamic stability, we investigate its complementarity with molecular docking, a method with a long and successful history of application in virtual screening.[16,17] Using the rDock software,[18] we find that docking scores have no correlation with W_{QB}, and good docking scorers are nearly as likely to present a low resistance to dissociation as the rest of the decoys (Figures 2C, 2D and Supplementary Figure 7). As such, molecular docking and dynamic undocking can be considered orthogonal (i.e. perfectly complementary) and the intersection between both techniques defines a region highly enriched in true ligands. We have also performed extensive calculations with other virtual screening tools (Glide docking, MMPBSA and MMGBSA re-scoring). The results, summarised in Supplementary Figures 8 and 9, confirm that DUck is complementary to all of them. In fact, as we obtain low W_{QB} values for many decoys with good scores by all other methods, DUck post-filtering delivers several fold improvement even when applied to a consensus list by two independent 'thermodynamic' approaches (Figures 2E, 2F and Supplementary Figure 10). These results support the idea that structural stability of the binding mode, just like good chemical complementarity, is a necessary – but not sufficient – condition for binding. By imposing both conditions simultaneously, we can multiply the effectiveness of structure-based virtual screening. At the same time,

using W_{QB} as a post-docking filter means that only the best-scoring subset of the virtual chemical collection needs to be reassessed by DUck simulations, thus improving computational efficiency.

Fragment discovery with in tandem docking-undocking calculations.

To demonstrate the power of the docking-undocking combination, we have applied the method prospectively for the identification of small molecules that bind the molecular chaperone, Heat Shock Protein 90KDa (Hsp90). This oncology target has been a test-bed and paradigm in fragment and structure-based drug design.[19] With hundreds of Hsp90-ligand complexes deposited in the Protein Data Bank (PDB), discovery of novel chemotypes is very challenging. We focused on fragment-like molecules, as this may be the most efficient way to discover new leads and to generate scaffold-hoping ideas.[20,21] A collection of 280000 fragment-sized molecules was docked to the ATP binding site of Hsp90. A diverse set of 139 molecules from the best 450 (top 0.16%) was then selected and each one was subjected to 100 DUck runs to obtain fully converged W_{QB} values (note that fewer DUck runs would have given similar results (Supplementary Figure 11)). The distribution of W_{QB} values (Figure 3A, Supplementary Figure 12) shows that even at the upper limit of the docking score distribution a large proportion of putative ligands present low resistance to dissociation, with 32%, 50% and 80% presenting W_{QB} below 3, 4 and 6 kcal/mol, respectively. We purchased all the molecules from the high stability set (W_{QB} > 6 kcal/mol) that were available (n=21). They were tested using three different ligand-observed Nuclear Magnetic Resonance (NMR) experiments, in the absence or presence of a known competitor to confirm that fragment hits bind at the target site.[19] Eight out of the 21 molecules (38%) were

confirmed as true hits (Table 1). Crucially, for the same system and screening method, the hit rate obtained with a general fragment screening library is 4.4%.[22] Therefore, the DUck-based virtual screening increases the efficiency by nearly an order of magnitude. This is similar to optimal virtual fragment screening results reported for other systems.[23]. In order to better assess the contribution of DUck to the success rate, we also purchased and collected data for 15 molecules from the medium stability set (W_{QB} between 3 and 6 kcal/mol) and 11 from the low stability set (W_{QB} < 3 kcal/mol). Only one molecule from these sets was a hit and, importantly, its W_{QB} value is very close to the upper threshold (5.6 kcal/mol). This confirms that DUck false negatives (i.e. active molecules with low W_{QB}) are rare, an ideal property for a screening method. Hit rates for the three categories are summarized in Figure 3B.

To assess the value of the hits as starting points, we have compared their chemical structures to existing Hsp90 ligands, finding low similarity in all cases (Table 1). Binding mode determination and analysis of the main interactions that define the chemical scaffold offers a more precise assessment of their novelty. Crystal structures for 3 of the fragment hits were determined by X-ray crystallography (Figure 4 and Supplementary Figure 13). This confirmed that the docking pose used as starting position for the DUck experiments was correct, particularly regarding the key interaction that was being monitored (side-chain of Asp93). Compound **1** is the most potent fragment hit (dissociation constant K_D=77μM) and has a ligand efficiency (LE) of 0.33 kcal/mol per non-hydrogen atom, similar to other Hsp90 fragment hits that have been evolved into very efficient lead compounds.[24] Many 2-aminopyrimidines have been described as Hsp90 ligands,[19]

confirming the potential of the fragment hit, but the relative lack of novelty would advise against using this fragment as starting point at this stage. Compound **2** is less potent (K_D=320μM) but equally efficient (LE=0.32) by virtue of having fewer atoms. In this case, the key interaction with Asp93 is mediated by an aminothiazole moiety, which is unprecedented and would constitute a good starting point to develop new chemical entities. Compound **3** (K_D=700μM; LE=0.25) belongs to the well-known family of resorcinol inhibitors, which includes the clinical candidate NVP-AUY922,[19] but provides an interesting example of scaffold hopping, where the oxime acts a bioisosteric replacement of the five-membered rings included as core scaffold in the patents. Compounds **4**, **5** and **6** also represent completely novel starting points, as their scaffold is unique amongst Hsp90 inhibitors. The binding mode could not be confirmed experimentally, but is likely correct because two independent methods deemed the molecules active based on the predicted geometry (Their predicted binding modes can be found in Supplementary Figure 14).

Conclusions

In summary, we have demonstrated that the concept of structural stability can be used very effectively in structure-based drug design, complementing the standard focus on binding free energy. Hydrogen-bonding groups in the active site are privileged structures to fix the ligand in place, particularly when they act as binding hot spots and can form water-shielded hydrogen bonds.[8] The work needed to break such interactions (W_{QB}) is very useful to detect true ligands even though it is a non-equilibrium property that is not expected to correlate with ΔG_{bind}. This

intriguing fact may reflect the nature of proteins, which have been designed to bind their natural ligands not only with high affinity and selectivity, but also forming structurally stable complexes. Thus, it will be important to test the approach on other types of supramolecular assemblies. Dynamic Undocking (DUck), a particular implementation of steered molecular dynamics, allows us to calculate W_{QB} in a very efficient manner. DUck can be used in combination with existing 'thermodynamic' approaches to multiply their effectiveness. The docking-undocking combination has proven particularly useful for virtual fragment screening, delivering novel, diverse and suitable starting points with a hit rate of 38%. At present, we focus on a single key hydrogen bond to estimate W_{QB}, which requires previous knowledge and has a critical impact on the outcome. Future investigations should address the extension of the method to multiple sites and other interaction types to improve performance and avoid reliance on extrinsic decisions. DUck inherits the intrinsic limitations of structure-based methods (e.g. protein flexibility, quality of the force-field) and may have some of its own (e.g. long range effects, steering conditions). Further tests will reveal its true potential, but considering that it is orthogonal to existing methods and computationally very efficient, we expect that it will be rapidly adopted by the structure-based drug design community and adapted to other biotechnological applications involving non-covalent complexes.

METHODS

Dynamic Undocking

Dynamic Undocking (DUck) is a particular type of Steered Molecular Dynamics (SMD),[25] where we force the rupture of an intermolecular hydrogen bond formed between a pre-defined interaction point in the receptor and a complementary atom in the ligand. Additionally, we use a model receptor that includes only the minimal subset of the protein necessary to preserve the local environment around the hydrogen bond that is being monitored. This transformation minimizes the influence of peripheral interactions, thus simplifying the dissociation pathway and facilitating convergence (Supplementary Figure 15). As an added bonus, it speeds up the calculations by a factor of 5 (Supplementary Table 2). The first and essential step is to identify an atom of reference in the protein, which must form a hydrogen bond with all (or most) known ligands. For well-known systems, like the ones used here, it can be identified from a structural superimposition of all the available protein-ligand complexes. On novel binding sites, it may be identified with a quantitative hot spot identification method.[26]. Then, the model receptor is generated from a representative 3D structure of the protein by selecting all residues with at least one atom within 6 Å of the atom of reference. The selection is visually inspected and, if needed, additional residues that are deemed necessary to preserve the local environment are included in the selection. Unselected residues are eliminated and truncated side chains are acetylated or N-methylated, as needed. Interstitial water molecules, if present, are preserved. The PDB codes, reference interaction points and the list of protein residues and water molecules for each system are listed in Supplementary Table 3. Given the model receptor

(protein chunk) and a set of ligands properly oriented (docking poses or superimposed X-ray geometries), a MOE[27] SVL script developed in house automatically performs the following steps: 1) Calculates AM1-BCC charges for the ligand.[28] 2) Assigns parm@Frosst[29] atom types and non-bonded parameters to the ligand. 3) Identifies the ligand atom that is hydrogen-bonded to the protein's reference atom (based on distance and type). 4) Writes input and execution files to carry out the MD simulations with AMBER[30]. 5) Calls AMBER's tLeap to generate valid topology and coordinate files for each individual receptor-ligand complex. For the protein, the AMBER force field 99SB is used. Each system is placed in a cuboid box spanning at least 12 Å more than the furthest atom in each direction. The box is then filled with TIP3 water molecules to create periodic boundary conditions. When needed, Na+ or Cl- ions are added to force the neutrality of the whole system. MD simulation conditions (where non-default) are as follows: 1) At all stages, harmonic restraints with a force constant of 1 kcal/mol·Å^2 are placed on all non-hydrogen atoms of the receptor to prevent structural changes. 2) Spontaneous rupture of the key hydrogen bond during non-steered simulations is prevented with a gradual restraint for distances beyond 3 Å (parabolic with k=1 kcal/mol·Å^2 between 3Å and 4Å and linear with k=10 kcal/mol·Å beyond 4 Å). 3) All equilibration and simulation steps were run using a Langevin thermostat with a collision frequency of 4 ps^{-1} and the cutoff for non-bonded interactions was set to 9Å. 4) Bonds involving hydrogen are constrained using SHAKE.[31] In order to equilibrate the system the following steps are executed: 1) Energy minimization for 1000 cycles. 2) Assignment of random velocities at 100K and gradual warming to 300K for 400 ps in the NVT ensemble. 3) Equilibration of the system for 1 ns in the NPT ensemble (1 atm, 300K). At this stage, the first SMD simulations can be

executed. We run two SMDs from the same restart file, but at different temperatures (300K and 325K) to ensure that the trajectories proceed differently. The SMD lasts 500 ps, during which time the distance between the key hydrogen bonds is steered from 2.5 Å to 5.0 Å (constant velocity of 5 Å/ns) with a spring constant of 50 kcal/mol·Å^2. We have tested slower velocities and the results are essentially unchanged (Supplementary Figure 16). The spring constant had little influence and on a limited test set we obtained essentially identical results in the range k=10 kcal/mol·Å^2 to k=1000 kcal/mol·Å^2. We have also investigated the importance of the specific reaction coordinate by using the closest contact between CDK2 Leu83:O and the ligand (instead of Leu83:N). The W_{QB} values obtained with these different atoms of reference (located only 3 Å apart) present a high correlation (r^2=0.75; Supplementary Figure 17). By contrast, when the atoms of reference involve completely different part of the ligand, the results are uncorrelated (Supplementary Figure 18). To generate diverse starting points for SMD trajectories, we perform 1ns unbiased MD simulation and repeat the process as many times as desired (e.g. 50ns unbiased MD simulations are needed to execute 100 SMD trajectories). All simulations were performed with Amber 12 adapted for running in GPUs and executed either in-house with NVIDIA GeForce TITAN X GPUs or at the Barcelona Supercomputing Center using NVIDIA Tesla M2090 GPUs. The simulations took 24 minutes (unbiased MD) or 30 minutes (SMD) of wallclock time per nanosecond (average values for the systems tested on the TITAN GPUs). Work profiles outputted by the SMD simulations are processed as explained in the main text to obtain W_{QB} values. Various methods could be used to obtain free energies from the SMD work, but they have strict convergence requirements, are computationally much more expensive and the results are only

valid if the reaction coordinate is mechanistically correct.[25] Instead, we simply assume that W_{QB} is an upper limit to the equivalent magnitude in free energy (ΔG_{QB}). In order to get as close as possible to ΔG_{QB}, we run multiple SMD replicas and take the overall lower W_{QB} as the representative value. Note that we have used very conservative settings, favouring sampling over computational efficiency. Based on convergence analysis (Supplementary Figures 6 and 11) and other tests, we propose the protocol shown in Supplementary Figure 19 for virtual screening. Less than one GPU hour per ligand would be necessary to discard approximately 80% of candidate ligands and produce a reasonable estimate of W_{QB} for the remaining ones. By comparison, a high-throughput implementation of MM-PBSA (1 ns of sampling) would require at least 3 GPU hours plus 20 CPU minutes per ligand.

Hsp90 virtual screening

A collection of 280000 purchasable fragment-sized molecules (<250 Da), were docked to the ATP binding site of Hsp90 with an optimized protocol, where the key hydrogen bond with Asp93 is enforced.[18] Next, we grouped the 1000 top scoring molecules into 400 clusters based on chemical similarity and visually inspected the top-scoring molecule within each cluster to select 139 molecules that were subjected to DUck simulations. Docking score was the main selection criterion, with 90 molecules originating from the top 200 and all of them within the top 450. Additional criteria included high predicted aqueous solubility and chemical diversity. The selected molecules were subjected to 100 DUck calculations. We divided the molecules in three categories according to their resistance to dissociation: weak ($W_{QB} < 3$; N=44; 32%), medium ($3 < W_{QB} < 6$; N=67; 48%) and

strong (W_{QB} > 6; N=28; 20%). We tested all the molecules that we could buy from the strong set. For comparison, we also purchased and tested 15 molecules of medium and 11 from the low stability sets. The chemical structures of the 47 compounds are shown in Supplementary Figure 12.

Screening by NMR

Identification of compounds which bind to the ATP site of Hsp90α was performed as described previously.[32,33] Briefly, a number of 1D ^{1}H NMR experiments (STD, water-LOGSY, relaxation filtered) were used to identify interactions between compounds and the protein; a potent competitor (PU3) was then added in order to block the ATP binding site. Compounds which bound and were then displaced were identified as interacting specifically with the protein.[34] Molecules active in all experiments were considered *bona fide* hits, while those giving a positive response in one or two experiments were considered unconfirmed hits because changes in NMR signal are not necessarily related to binding. All NMR experiments were performed on a BrukerAvIII HD 600 MHz NMR spectrometer at 298K; pulse sequences included an excitation sculpting module in order to suppress bulk water. Samples contained 500 μM ligand and 10 μM Hsp90α in 20mM tris pH 7.5, 50mM NaCl 1mM freshly prepared DTT and contained 10% D_2O.

X-Ray crystallographic studies

Protein was produced and crystallized as previously described.[35] For the successful crystals, data were collected at 100K on an in-house Bruker D8 Venture TXS Generator with a Bruker Photo 100 detector and were subsequently processed using SAINT & SADABS. The crystals belong to the space groups I222.

386 The structures were solved by molecular replacement using a previously solved
387 Hsp90α protein model (PDB code: 1UY6; PU3 ligand and solvent removed) and the
388 program AMoRe.[36] Twenty cycles of rigid-body then restrained refinement were
389 carried out using the refinement program REFMAC5[37] followed by model building
390 and solvent addition using the molecular graphics program COOT.[38] The progress
391 of the refinement was assessed using R_{free} and the conventional R factor. Once
392 refinement was completed the structures were validated using various programs
393 from the CCP4i package.[39] Full data collection and refinement statistics are
394 presented in Supplementary Table 4.
395
396 Methodological details concerning the creation of the datasets, molecular docking,
397 MMPBSA and MMGBSA calculations, and surface plasmon resonance experiments
398 are provided as Supplementary Information.
399
400
401
402

ACKNOWLEDGEMENTS

We thank Carles Galdeano for helpful discussions and manuscript revision. We thank the Barcelona Supercomputing Center for access to computational resources. This work was financed by the Spanish Ministerio de Economia (SAF2012-33481, SAF2015-68749-R), the Catalan government (2014 SGR 1189) and the ICREA Academia program (FJL).

Correspondence and requests for materials should be addressed to X. B.

Author contributions

F.J.L, R.H. and X.B. conceived the overall strategy of the study. P.S. and X.B. conceived and implemented the DUck approach. S.R.C. and X.B. carried out and analysed all computational work. B.D. performed NMR experiments. L.B. performed X-ray crystallography experiments. N.M. performed SPR experiments. All authors discussed the results, designed experiments and wrote the paper.

Code Availability statement

A step-by-step guide on how to prepare, execute and analyse DUck simulations, along with scripts used to automate the process can be found on the following website: http://www.ub.edu/bl/undocking

REFERENCES

1. Kuhnert, M. *et al.* Tracing Binding Modes in Hit-to-Lead Optimization: Chameleon-Like Poses of Aspartic Protease Inhibitors. *Angew. Chem. Int. Ed. Engl.* **54,** 2849–2853 (2015).
2. Krohn, A., Redshaw, S., Ritchie, J. C., Graves, B. J. & Hatada, M. H. Novel binding mode of highly potent HIV-proteinase inhibitors incorporating the (R)-hydroxyethylamine isostere. *J. Med. Chem.* **34,** 3340–3342 (1991).
3. Smith, L. J., Gunsteren, W. F. Van & Allison, J. R. Multiple binding modes for palmitate to barley lipid transfer protein facilitated by the presence of proline 12. *Protein Sci.* **22,** 56–64 (2013).
4. Bissantz, C., Kuhn, B. & Stahl, M. A Medicinal Chemist's Guide to Molecular Interactions. *J. Med. Chem.* 5061–5084 (2010). doi:10.1021/jm100112j
5. Klebe, G. Applying thermodynamic profiling in lead finding and optimization. *Nat. Rev. Drug Discov.* **14,** 95–110 (2015).

6. Ferenczy, G. G. & Keserű, G. M. Thermodynamics of fragment binding. *J. Chem. Inf. Model.* **52,** 1039–45 (2012).

7. Kozakov, D. *et al.* Ligand deconstruction: Why some fragment binding positions are conserved and others are not. *Proc. Natl. Acad. Sci. U. S. A.* **112,** E2585-2594 (2015).

8. Schmidtke, P., Luque, F. J., Murray, J. B. & Barril, X. Shielded hydrogen bonds as structural determinants of binding kinetics: application in drug design. *J. Am. Chem. Soc.* **133,** 18903–10 (2011).

9. Colizzi, F., Perozzo, R., Scapozza, L., Recanatini, M. & Cavalli, A. Single-molecule pulling simulations can discern active from inactive enzyme inhibitors. *J. Am. Chem. Soc.* **132,** 7361–71 (2010).

10. Noble, M. E. M., Endicott, J. a & Johnson, L. N. Protein kinase inhibitors: insights into drug design from structure. *Science* **303,** 1800–5 (2004).

11. Anderson, D. R. *et al.* Benzothiophene inhibitors of MK2. Part 1: structure-activity relationships, assessments of selectivity and cellular potency. *Bioorg. Med. Chem. Lett.* **19,** 4878–81 (2009).

12. Filippakopoulos, P. & Knapp, S. Targeting bromodomains: epigenetic readers of lysine acetylation. *Nat. Rev. Drug Discov.* **13,** 337–356 (2014).

13. Ember, S. W. J. *et al.* Acetyl-lysine binding site of bromodomain-containing protein 4 (BRD4) interacts with diverse kinase inhibitors. *ACS Chem. Biol.* **9,** 1160–1171 (2014).

14. Mysinger, M. M., Carchia, M., Irwin, J. J. & Shoichet, B. K. Directory of useful decoys, enhanced (DUD-E): Better ligands and decoys for better benchmarking. *J. Med. Chem.* **55,** 6582–6594 (2012).

15. Rask-Andersen, M., Almén, M. S. & Schiöth, H. B. Trends in the exploitation of novel drug targets. *Nat. Rev. Drug Discov.* **10,** 579–90 (2011).

16. Shoichet, B. K. Virtual screening of chemical libraries. *Nature* **432,** 862–5 (2004).

17. Brooijmans, N. & Kuntz, I. D. Molecular recognition and docking algorithms. *Annu. Rev. Biophys. Biomol. Struct.* **32,** 335–73 (2003).

18. Ruiz-Carmona, S. *et al.* rDock: A Fast, Versatile and Open Source Program for Docking Ligands to Proteins and Nucleic Acids. *PLoS Comput. Biol.* **10,** e1003571 (2014).

19. Roughley, S., Wright, L., Brough, P., Massey, A. & Hubbard, R. E. Hsp90 inhibitors and drugs from fragment and virtual screening. *Top. Curr. Chem.* **317,** 61–82 (2012).

20. Hajduk, P. J. & Greer, J. A decade of fragment-based drug design: strategic advances and lessons learned. *Nat. Rev. Drug Discov.* **6,** 211–9 (2007).

21. Joseph-McCarthy, D., Campbell, A. J., Kern, G. & Moustakas, D. Fragment-based lead discovery and design. *J. Chem. Inf. Model.* **54,** 693–704 (2014).

22. Chen, I.-J. & Hubbard, R. E. Lessons for fragment library design: analysis of

484 output from multiple screening campaigns. *J. Comput. Aided. Mol. Des.* 603–
485 620 (2009). doi:10.1007/s10822-009-9280-5

486 23. Teotico, D. G. *et al.* Docking for fragment inhibitors of AmpC beta-lactamase.
487 *Proc. Natl. Acad. Sci. U. S. A.* **106,** 7455–7460 (2009).

488 24. Murray, C. W. *et al.* Fragment-based drug discovery applied to Hsp90.
489 Discovery of two lead series with high ligand efficiency. *J. Med. Chem.* **53,**
490 5942–55 (2010).

491 25. Chipot, C. & Pohorille, A. *Free Energy Calculations Theory and Applications in*
492 *Chemistry and Biology*. *Free Energy Calculations Theory and Applications in*
493 *Chemistry and Biology* (Springer Berlin Heidelberg, 2007).

494 26. Alvarez-Garcia, D. & Barril, X. Molecular simulations with solvent
495 competition quantify water displaceability and provide accurate interaction
496 maps of protein binding sites. *J. Med. Chem.* **57,** 8530–9 (2014).

497 27. Chemical Computing Group Inc. Molecular Operating Environment (MOE),
498 2014.09. (2015).

499 28. Jakalian, A., Jack, D. B. & Bayly, C. I. Fast, efficient generation of high-quality
500 atomic charges. AM1-BCC model: II. Parameterization and validation. *J.*
501 *Comput. Chem.* **23,** 1623–41 (2002).

502 29. Bayly, C. I., McKay, D. & Truchon, J. F. An Informal AMBER Small Molecule
503 Force Field: parm@Frosst. (2011).

504 30. Case, D. A. *et al.* AMBER 12. (2012).

505 31. Ryckaert, J.-P., Ciccotti, G. & Berendsen, H. J. C. Numerical integration of the
506 cartesian equations of motion of a system with constraints: molecular
507 dynamics of n-alkanes. *J. Comput. Phys.* **23,** 327–341 (1977).

508 32. Brough, P. a *et al.* Combining hit identification strategies: fragment-based
509 and in silico approaches to orally active 2-aminothieno[2,3-d]pyrimidine
510 inhibitors of the Hsp90 molecular chaperone. *J. Med. Chem.* **52,** 4794–809
511 (2009).

512 33. Baurin, N. *et al.* Design and characterization of libraries of molecular
513 fragments for use in NMR screening against protein targets. *J. Chem. Inf.*
514 *Comput. Sci.* **44,** 2157–2166 (2004).

515 34. Davis, B. in *Protein-Ligand Interactions: Methods and Applications* (eds.
516 Williams, M. A. & Daviter, T.) **1008,** 389–413 (Springer Science+Business
517 Media, 2013).

518 35. Wright, L. *et al.* Structure-activity relationships in purine-based inhibitor
519 binding to HSP90 isoforms. *Chem. Biol.* **11,** 775–85 (2004).

520 36. Navaza, J. AMoRe: an automated package for molecular replacement. *Acta*
521 *Crystallogr. Sect. A Found. Crystallogr.* **50,** 157–163 (1994).

522 37. Murshudov, G. N., Vagin, A. A. & Dodson, E. J. Refinement of macromolecular
523 structures by the maximum-likelihood method. *Acta Crystallogr. Sect. D Biol.*
524 *Crystallogr.* **53,** 240–255 (1997).

525 38. Emsley, P. & Cowtan, K. Coot: model-building tools for molecular graphics.
526 *Acta Crystallogr. Sect. D Biol. Crystallogr.* **60,** 2126–2132 (2004).

527 39. Collaborative, C. P. & others. The CCP4 suite: programs for protein
528 crystallography. *Acta Crystallogr. D. Biol. Crystallogr.* **50,** 760 (1994).

529

TABLES

Table 1. Summary of results for the 9 Hsp90 NMR Class 1 hits. Chemical structures of all compounds are shown in Supplementary Table 1.

ID	MW	Docking	DUck	SPR Kd (mM)	PDB Sim[b]	ChEMBL Sim.[b]
		Score (Rank[a])	Score (Rank[a])			
1*	248.7	-25.0 (79)	9.1 (10)	77	2XDX (0.37)	CHEMBL 1340447 (0.44)
2*	221.3	-25.0 (73)	8.2 (11)	320	2WI6 (0.29)	CHEMBL 1536318 (0.54)
3*	230.2	-26.7 (19)	11.3 (1)	700	4EFU (0.32)	CHEMBL 1458840 (0.51)
4	240.3	-26.4 (22)	7.4 (16)	730	3WHA (0.29)	CHEMBL 1542436 (0.37)
5	165.2	-23.8 (128)	8.1 (12)	-	4EFT (0.27)	CHEMBL 1313412 (0.28)
6	206.3	-23.3 (138)	9.5 (5)	-	3HHU (0.42)	CHEMBL 2103879 (0.42)
7	236.3	-25.4 (51)	7.8 (15)	-	3B24 (0.31)	CHEMBL 1375884 (0.36)
8	224.7	-25.3 (58)	7.0 (22)	-	2XDX (0.35)	CHEMBL 1383799 (0.37)
22	237.3	-28.3 (2)	5.6 (33)	-	3O0I (0.27)	CHEMBL 1834092 (0.33)

*Xray structure solved [a]Position within the list of 149 molecules that were evaluated with DUck. [b]Hsp90 structure in the PDB or compound with Hsp90 activity in ChEMBL (as of 23/03/2016) with the closest similarity to the fragment hit. Similarity (values in parentheses) was calculated with Open Babel using the FP2 fingerprint.

FIGURE CAPTIONS

Figure 1. Calculation of W_{QB}. **a**. The receptor is idealized as a model system containing only the local environment around a key intermolecular hydrogen bond. **b**. Representative work profiles obtained from dynamic undocking simulations for a strong (black) and a weak (grey) ligand. The quasi-bound state is defined as the point with the highest energy relative to the ideal hydrogen bond geometry.

Figure 2. Application of the quasi-bound approximation to ligand ranking. **a.** Distribution of W_{QB} values of potent CDK2 ligands (IC_{50} < 1μM; dark grey), weak CDK2 ligands (IC_{50} > 1μM; light grey) and non-binding decoys (black). Points indicate population values, from which the smooth lines are extrapolated. **b.** ROC curves for the CDK2 (black), A2AR (red) and Trypsin (green) DUD sets. Plotted results correspond to 2 DUck runs per ligand. AUC values are shown in Supplementary Figure 6. **c.** Docking score vs. W_{QB} values for active (red) and inactive (black or gray) compounds in the CDK2 retrospective virtual screening dataset. The quadrant in orange highlights the area corresponding to top 25% docking score and top 25% W_{QB} values, where optimal enrichment factors (EF) are achieved. **d.** For the same set, distribution of W_{QB} values for the active compounds (red), all decoys (black) and decoys in the top 25% docking score (gray). **e.** Distribution of W_{QB} values of CDK2 actives (red) and decoys (gray) ranked in the top 25% by two independent docking programs (rDock and Glide). **f.** Distribution of W_{QB} values of CDK2 actives (red) and decoys (gray) ranked in the top 25% both by MMPBSA and the rDock docking program.

Figure 3. Additional analyses of the prospective application of DUck in Hsp90. **a**. Distribution of W_{QB} values for 139 top docking scorers (pale gray), 47 compounds within this set that were purchased (dark gray), and the 9 compounds detected as active. **b**. Pie charts showing the hit rates for the set of compounds with high W_{QB} (top), medium W_{QB} (middle) and low W_{QB} (bottom). The area in black corresponds to bona fide hits, dark gray represents compounds that give a positive signal in 1 or 2 NMR experiments, pale gray corresponds to inactive compounds. Labels indicate the number of compounds of each class. Chemical structures are shown in Supplementary Figure 12.

585 **Figure 4.** Experimental (grey) and predicted (orange) binding modes of the
586 fragment hits. **a.** Compound **1**, the RMSD of the whole molecule is 2.58 Å due to a
587 conformational change of the protein next to the p-toluene ring. The pyridine ring
588 and bonded atoms, where the key interaction occur, have a RMSD of 0.54 Å **b.**
589 Compound **2** has a RMSD of 0.54 Å **c.** Compound **3** has a RMSD of 1.55 Å, all
590 hydrogen bond interactions are preserved.

591

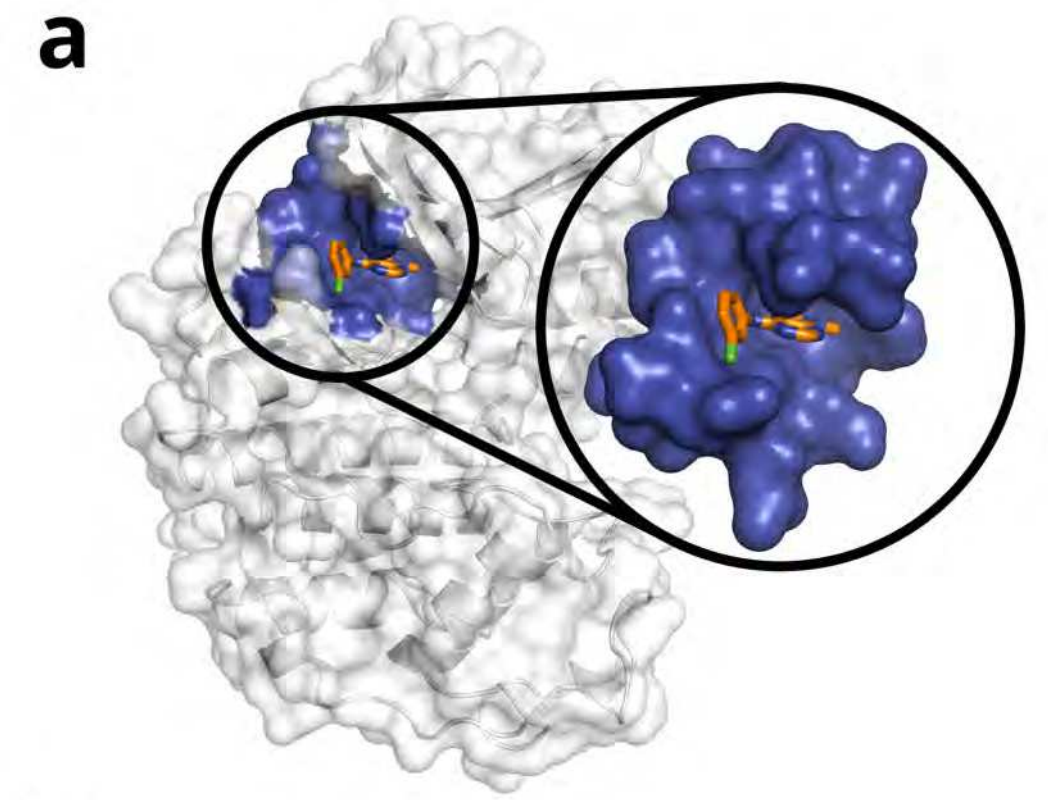
a

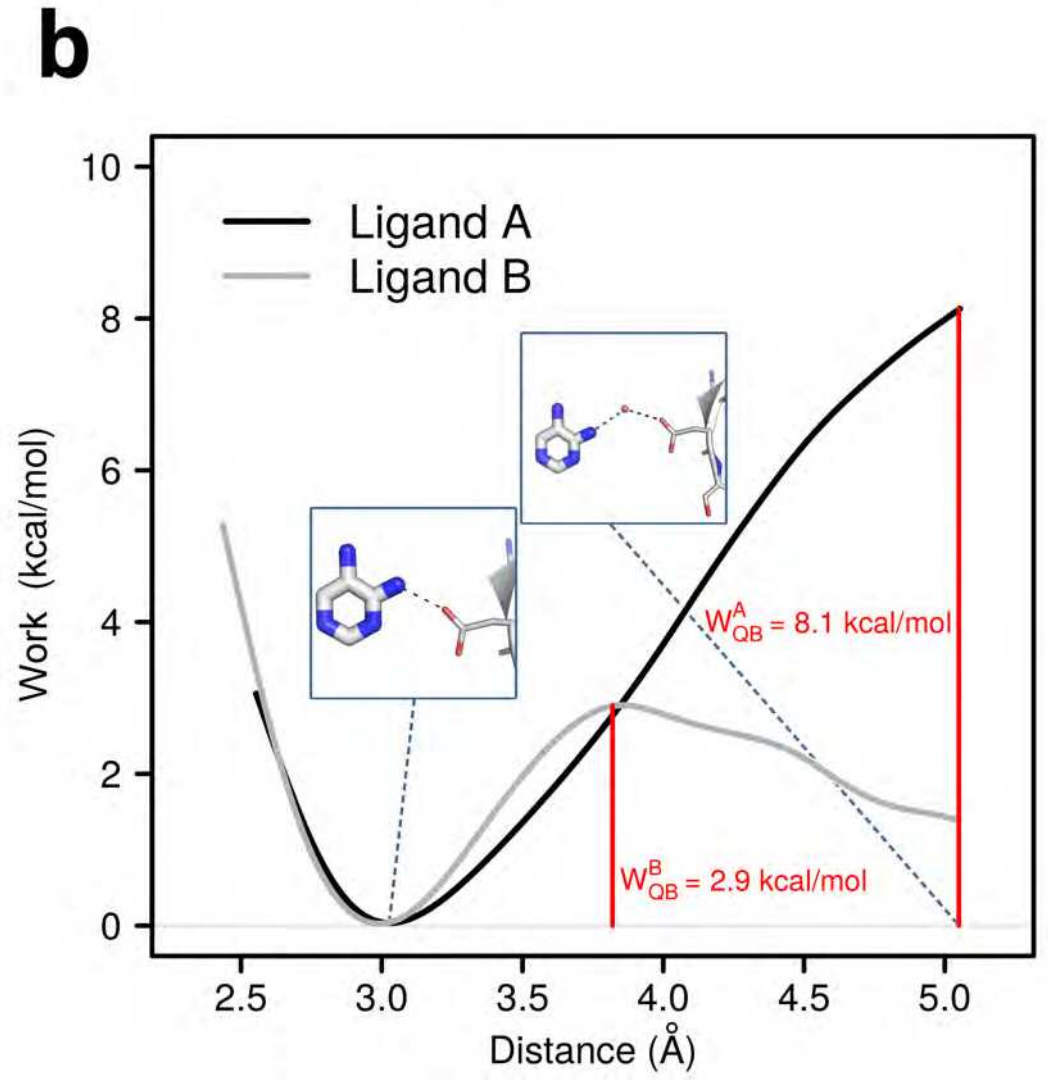
b
Ligand A
Ligand B
Work (kcal/mol)
Distance (Å)
10
8
6
4
2
0
2.5
3.0
3.5
4.0
4.5
5.0
W^{A}_{QB} = 8.1 kcal/mol
W^{B}_{QB} = 2.9 kcal/mol

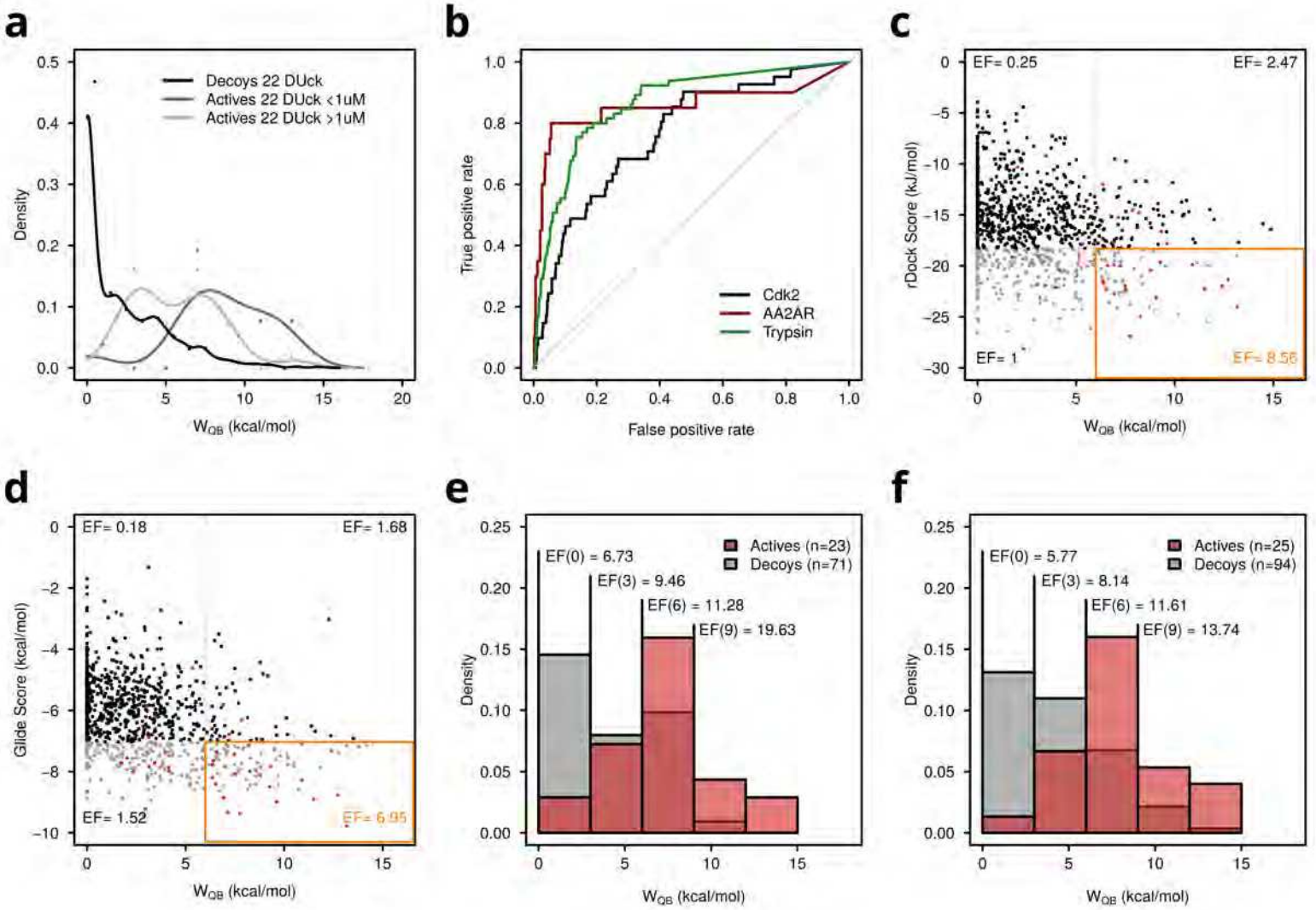
a
Decoys 22 DUck
Actives 22 DUck <1uM
Actives 22 DUck >1uM
Density
W_OB (kcal/mol)
b
Cdk2
AA2AR
Trypsin
True positive rate
False positive rate
c
EF= 0.25
EF= 2.47
EF= 1
EF= 8.56
rDock Score (kJ/mol)
W_OB (kcal/mol)
d
EF= 0.18
EF= 1.68
EF= 1.52
EF= 6.95
Glide Score (kcal/mol)
W_OB (kcal/mol)
e
Actives (n=23)
Decoys (n=71)
EF(0) = 6.73
EF(3) = 9.46
EF(6) = 11.28
EF(9) = 19.63
Density
W_OB (kcal/mol)
f
Actives (n=25)
Decoys (n=94)
EF(0) = 5.77
EF(3) = 8.14
EF(6) = 11.61
EF(9) = 13.74
Density
W_OB (kcal/mol)

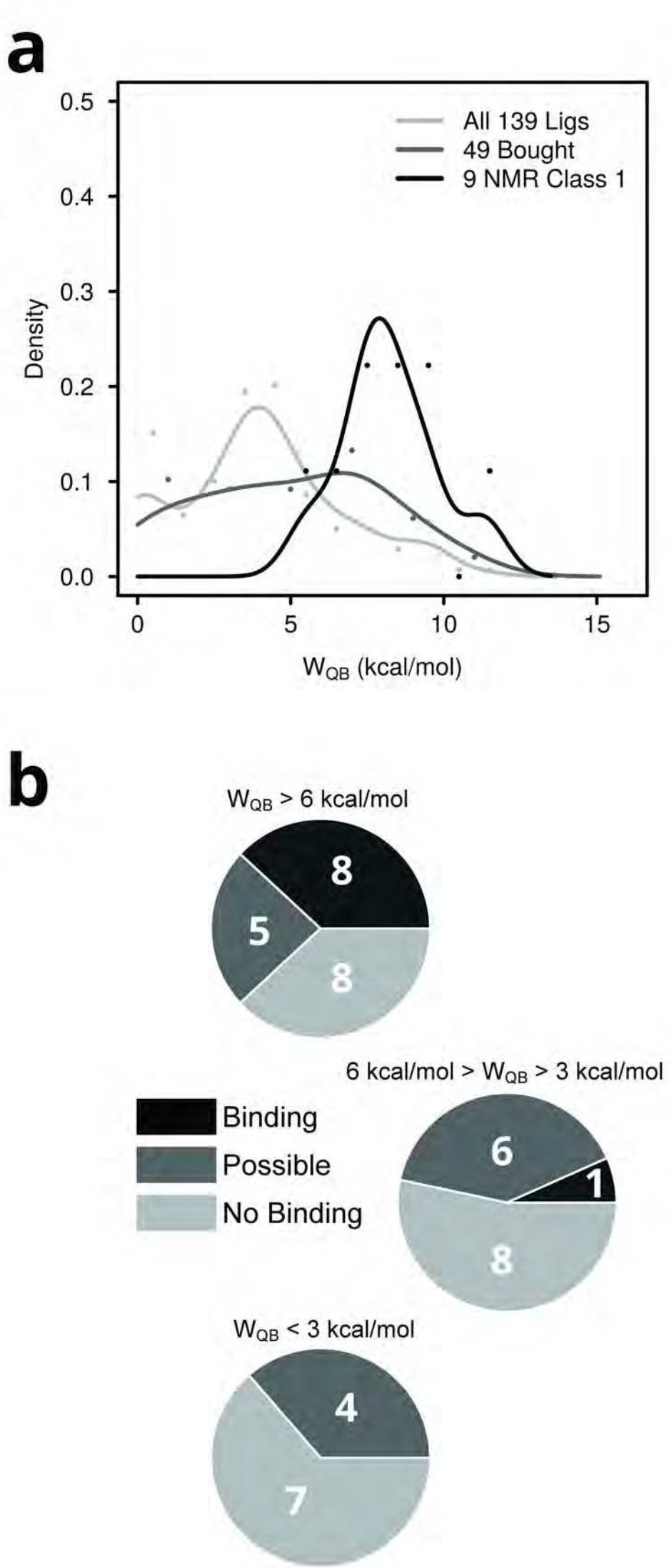
a
All 139 Ligs
49 Bought
9 NMR Class 1
Density
0.0
0.1
0.2
0.3
0.4
0.5
0
5
10
15
W_{QB} (kcal/mol)
b
W_{QB} > 6 kcal/mol
8
5
8
6 kcal/mol > W_{QB} > 3 kcal/mol
Binding
Possible
No Binding
6
1
8
W_{QB} < 3 kcal/mol
4
7

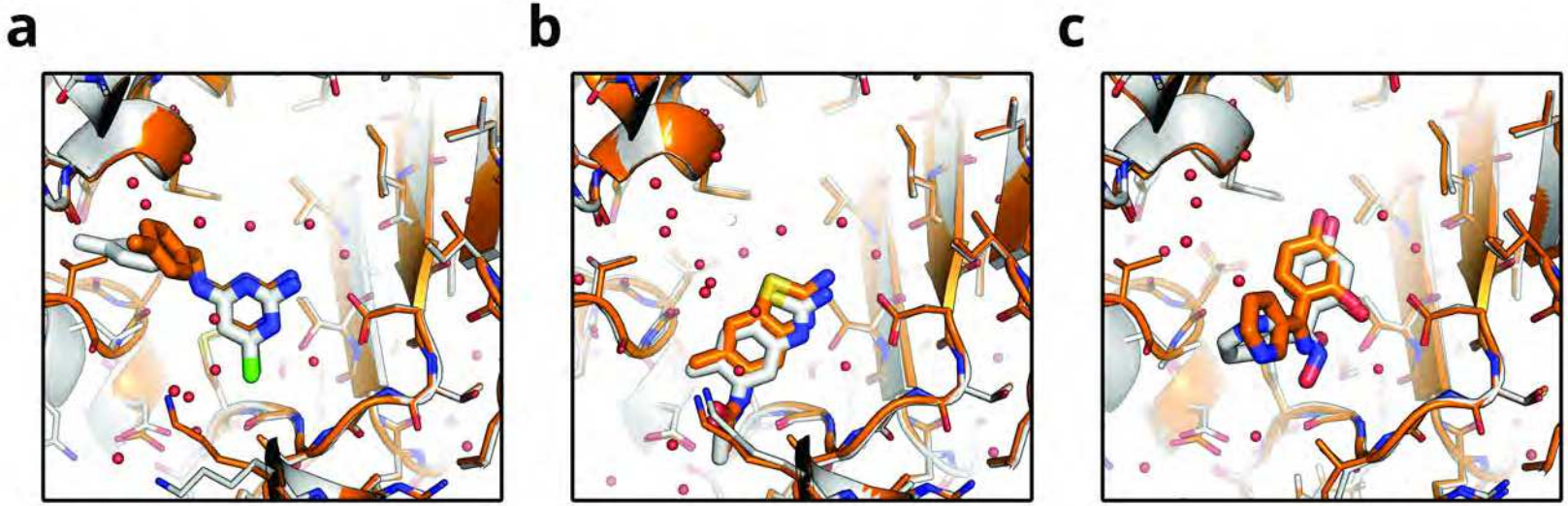
a
b
c

Supplementary Information

Dynamic Undocking and the Quasi-Bound State as Tools for Drug Design

Sergio Ruiz-Carmona, Peter Schmidtke, F. Javier Luque, Lisa Baker, Natalia Matassova, Ben Davis, Stephen Roughley, James Murray, Rod Hubbard, Xavier Barril

INDEX

SUPPLEMENTARY METHODS

Datasets

When possible, datasets were geared towards fragment-sized ligands because they present more scaffold diversity, make fewer peripheral interactions that could mask the main interactions and because Fragment-Based Drug Discovery (FBDD) approaches are increasingly important as hit identification strategy.[1,2] For CDK2, all ligands with molecular weight below 300 Da and known binding affinity (IC50) were extracted from the PDB.[3] To increase the diversity of the dataset, all ligands were clustered at 75% similarity using the MACCS fingerprints as implemented in MOE (Chemical Computing Group Inc., 2015) and only the centroids were used to define the active set. The composition of the dataset is described in Supplementary Table 5. It should be noted that this is a noisy dataset because data sources are very heterogeneous and IC_{50} values have an indirect relationship with dissociation constants.[4] As such, it should only be used to detect trends. In order to assess the significance of the correlation, we have also investigated the correlation between IC_{50} and molecular weight (Supplementary Figure 20). For retrospective VS experiments, a pool of 30 decoys per active fragment was obtained with the DUD-E decoy generator,[5] which puts together a set of putatively inactive molecules with physicochemical properties very similar to active ones. For BRD4, as it was designed to study the correlation between experimental binding affinity and W_{QB}, only the ligands with known binding mode and measured IC_{50} or K_D were considered (relationship with molecular weight reported in Supplementary Figure 21). The crystal structure of each ligand-protein complex was obtained from PDB and used as input for subsequent calculations. The composition of the dataset is described in Supplementary Table 6. In the case of AA2AR, as there are few structures in the PDB, the active fragments were taken from the DUD-E benchmark set.[5] The rest of the procedure is the same as described for CDK2. For Trypsin, we found that few ligands have a low molecular weight so we did not filter by size. Instead, a random subset of 2000 actives and decoys was selected from DUD-E. In the case of Hsp90, all candidate molecules originate from a unified collection generated in house from the commercial libraries of five preferred vendors (Specs, Enamine, Life Chemicals, Princeton Biomoleculars and Asinex). In this case we set an upper limit of 250 Da, obtaining 280000 candidate fragments. All ligands were

prepared for docking using Schrödinger's Ligprep[6]with the following options different than default: neutralize and ionize at pH 7 with a threshold of +- 1 with a maximum of 6 tautomers and 8 stereoisomers generated.

Molecular Docking with rDock

For CDK2, AA2AR and Trypsin, the 3D structure used to define the receptor was obtained from the DUD-E benchmark set.[5] MOE[7] was used to generate mol2 files that can be read by rDock, our docking engine.[8] For Hsp90, we use the same cavity definition and docking protocol described previously.[8] In all systems, pharmacophoric restraints were used to ensure that the key interaction point was matched by every molecule in the dataset, as defined in Supplementary Table 3. rDock was run with the default parameters for standard docking. 50 individual docking processes were executed per ligand, thus ensuring that the lowest-energy binding mode is identified. The best-scoring solution is accepted as the putative binding mode. Ligands that do not fulfill the pharmacophore are identified by the restraint penalty and eliminated from the dataset (i.e. not considered in the ROC curves or any other analysis).

Molecular Docking with Glide

In order to demonstrate that our methodology provides an advantage regardless of the docking program used, we also run CDK2, AA2R and trypsin systems with Glide.[9] The generation of the cavity with Glide was performed using coordinates defined as in rDock docking and default parameters. Pharmacophoric restraints were defined to force all ligands to make a hydrogen bond as defined in Supplementary Table 3. Glide docking was run with default parameters and with pharmacophoric restraints (Supplementary Figures 22, 23 and 24). The best docking pose for each ligand was selected and used as input for DUck.

MMGBSA and MMPBSA

MMGBSA and MMPBSA calculations using AMBER12 software were also performed and compared against the rest of methods. Each ligand was simulated for 5 ns with the full size receptor of CDK2 using the same MD configuration defined in the section above (Supplementary Figures 24 and 25). For each

simulation, a total of 25 snapshots separated by 200 ps were used and the free energies were averaged over the ensemble of conformations. All the calculations were performed with default parameters with the exception of the following: the GB model used is one of the developed by Onufriev et al.[10] (igb=2) and the atomic radii are set up according to the topology (radiopt=0).

Surface plasmon resonance

Surface plasmon resonance (SPR) experiments have been done mainly as described before.[11,12] All measurements were performed on a Biacore T200 instrument (Biacore GE Healthcare) at 20°C on Series S NTA chips. 25 mM HEPES pH7.4, 175 mM NaCl, 0.01% P-20, 0.025mM EDTA and 1% DMSO was used as a running buffer. HSP90 protein was produced as described previously. Chip surface was generated with multi-His-tagged Hsp90 protein as in reference.[11] The sensor surface was regenerated by 0.35 M EDTA and 45% DMSO with additional 60 sec injections of 0.1 mg/mL trypsin and 0.5 M imidazole. In some experiments, the protein was further stabilized on NTA surface by covalent amine coupling as advised by manufacturer. Screening of fragments was conducted in dose response titrations of nine two-fold diluted experimental points with the top concentration of 500 μM. Each fragment has been tested at least three times. Data processing was performed using BIAevaluation 2.1 (Biacore GE Healthcare Bio-SciencesCorp) or Scrubber2 (BioLogic) software. Sensorgrams were double referenced prior to global fitting of the concentration series to a Steady State Affinity model. Representative sensorgrams are shown in Supplementary Figure 26.

SUPPLEMENTARY REFERENCES

1. Joseph-McCarthy, D., Campbell, A. J., Kern, G. & Moustakas, D. Fragment-based lead discovery and design. *J. Chem. Inf. Model.* **54,** 693–704 (2014).
2. Hajduk, P. J. & Greer, J. A decade of fragment-based drug design: strategic advances and lessons learned. *Nat. Rev. Drug Discov.* **6,** 211–9 (2007).
3. Berman, H. M. *et al.* The Protein Data Bank. *Nucleic Acids Res.* **28,** 235–242 (2000).
4. Klebe, G. Applying thermodynamic profiling in lead finding and optimization. *Nat. Rev. Drug Discov.* **14,** 95–110 (2015).
5. Mysinger, M. M., Carchia, M., Irwin, J. J. & Shoichet, B. K. Directory of useful decoys, enhanced (DUD-E): Better ligands and decoys for better benchmarking. *J. Med. Chem.* **55,** 6582–6594 (2012).
6. Schrödinger. LigPrep, version 2.9. *Schrödinger, LLC* (2014).
7. Chemical Computing Group Inc. Molecular Operating Environment (MOE), 2014.09. (2015).
8. Ruiz-Carmona, S. *et al.* rDock: A Fast, Versatile and Open Source Program for Docking Ligands to Proteins and Nucleic Acids. *PLoS Comput. Biol.* **10,** e1003571 (2014).
9. Friesner, R. a *et al.* Glide: a new approach for rapid, accurate docking and scoring. 1. Method and assessment of docking accuracy. *J. Med. Chem.* **47,** 1739–49 (2004).
10. Onufriev, A., Bashford, D. & Case, D. A. Exploring Protein Native States and Large-Scale Conformational Changes with a Modified Generalized Born Model. *Proteins Struct. Funct. Genet.* **55,** 383–394 (2004).
11. Meiby, E. *et al.* Fragment screening by weak affinity chromatography: comparison with established techniques for screening against HSP90. *Anal. Chem.* **85,** 6756–66 (2013).
12. Murray, J. B., Roughley, S. D., Matassova, N. & Brough, P. a. Off-rate screening (ORS) by surface plasmon resonance. An efficient method to kinetically sample hit to lead chemical space from unpurified reaction products. *J. Med. Chem.* **57,** 2845–2850 (2014).
13. Anderson, D. R. *et al.* Benzothiophene inhibitors of MK2. Part 1: structure-activity relationships, assessments of selectivity and cellular potency. *Bioorg. Med. Chem. Lett.* **19,** 4878–81 (2009).
14. O'Boyle, N. M. *et al.* Open Babel: An Open chemical toolbox. *J. Cheminform.* **3,** (2011).

SUPPLEMENTARY FIGURES

Supplementary Figure 1

Graphical representation of the quasi-bound state in relation to the dissociation process. The macroscopic constants describing the behavior of a non-covalent complex are determined by the relative free energies of three states (bound, transition state and unbound). States in-between are theoretically irrelevant, so molecules 1, 2 and 3 would have the same kinetic and thermodynamic constants. The Quasi-bound state is merely designed to probe the slope around the bound state, obtaining an approximation to the structural stability of the binding mode. We find that true ligands are more likely to have a profile like 1, whereas many decoys have profiles similar to 2 or 3.

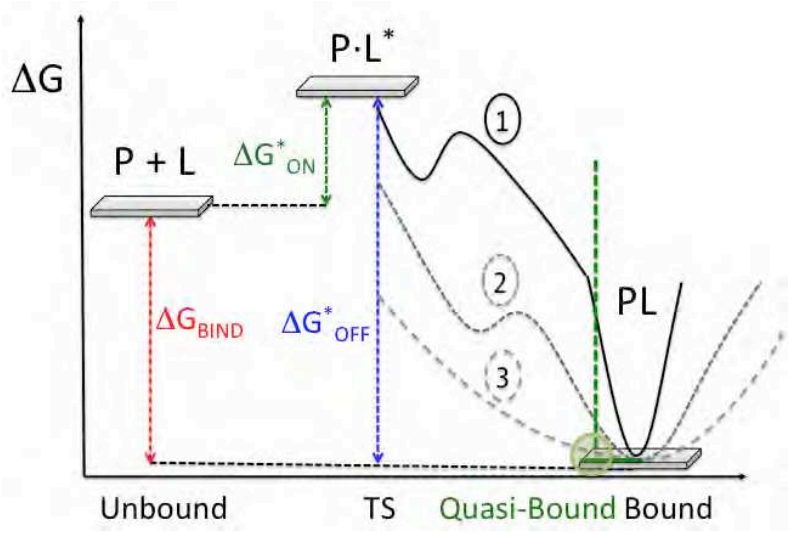

Supplementary Figure 2

W_{QB} values vs. experimentally determined activities (expressed as Log(IC_{50})), for a set of 41 Fragment-like CDK2 ligands taken from the PDB. Ligand 3FZ1 is shown in red and not included in the correlation. As shown below, this ligand does not fulfill the condition of using the hinge region as attachment point.

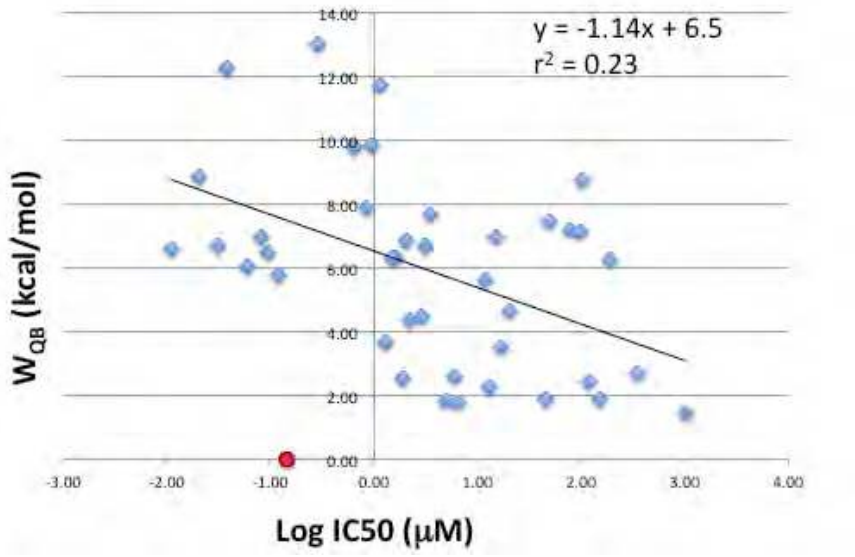

Supplementary Figure 3

Distribution of W_{QB} values as a function of binding affinity (IC_{50}), for the CDK2 (top) and BRD4 set (bottom). Compounds with the same binding affinity present a wide distribution of W_{QB} values, but there is a tendency towards higher values for more potent compounds. Most notably, very low W_{QB} values are rare for potent ligands.

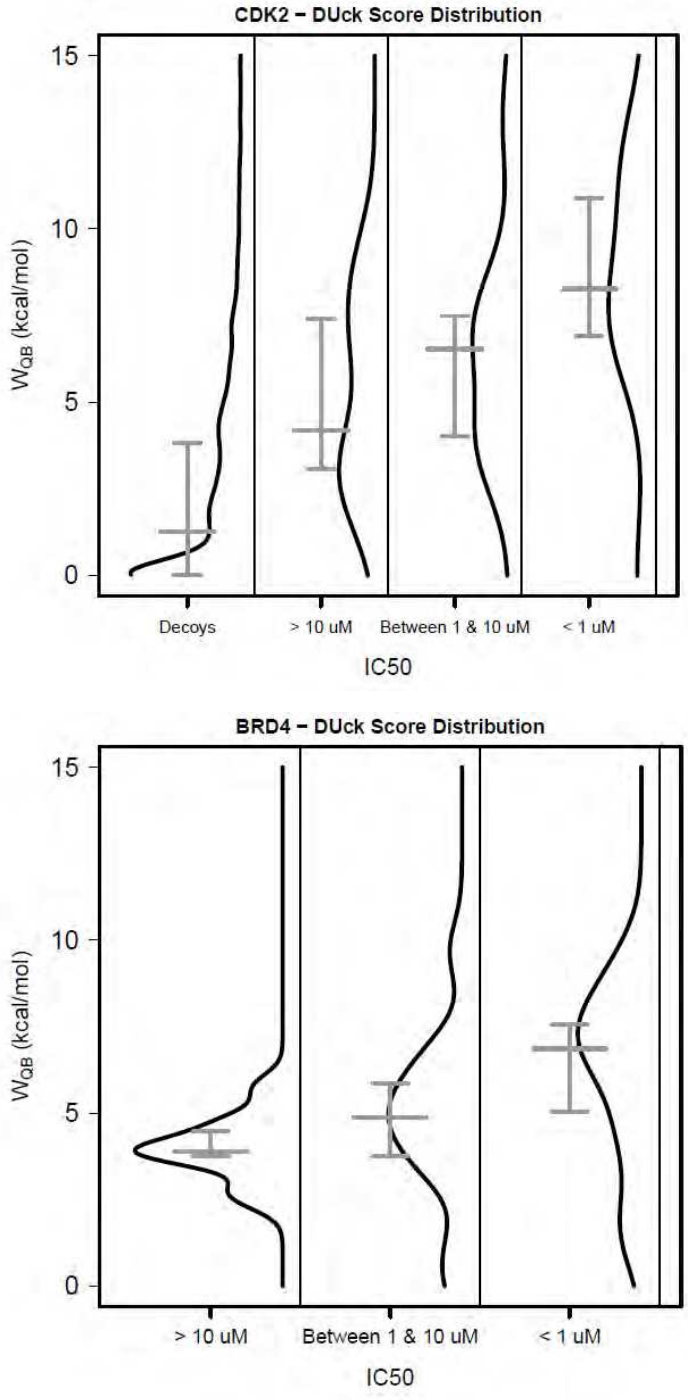

Supplementary Figure 4

Binding mode of ligand in PDB structure 3FZ1. This ligand is unusual because its interaction with the hinge region is labile. Structural and SAR data confirms that this interaction is not important for potency.[13] Instead, this ligand forms two charge-reinforced hydrogen bonds with Nζ of Lys33 and Oδ1 of Asn132, from which it draws structural stability (W_{QB} = 10.50 kcal/mol; Supplementary Figure 18). Note that the IC_{50} reported in the PDB for this compound is wrong. The correct value is 146 nM.[13]

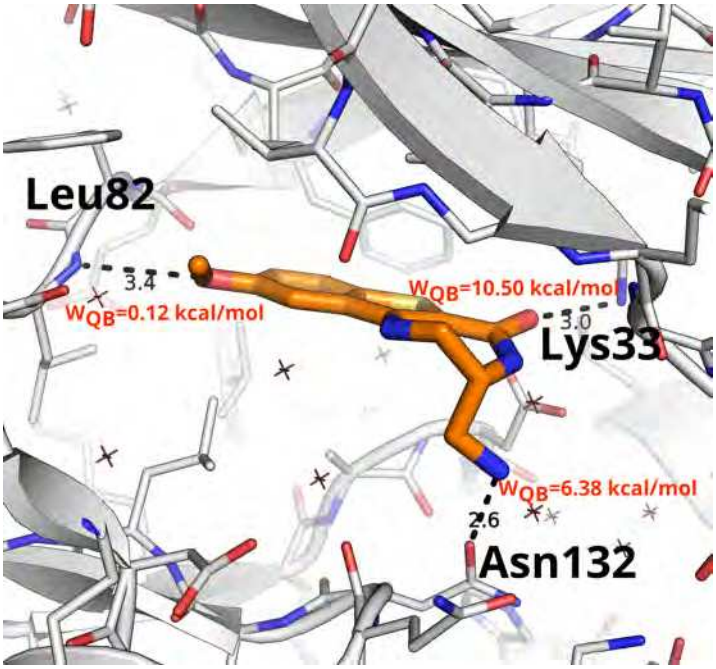

Supplementary Figure 5

W_{QB} values vs. experimentally determined activities (expressed as Log(IC_{50})), for a set of 30 BRD4 ligands taken from the PDB. The points in red have not been included in the correlation. They correspond to three kinase inhibitors that bind to BRD4 as an unintended secondary target and present extremely low resistance to breaking the interaction with Nδ2 of Asn120 (PDB codes 4O74, 4O77 & 4O7E).

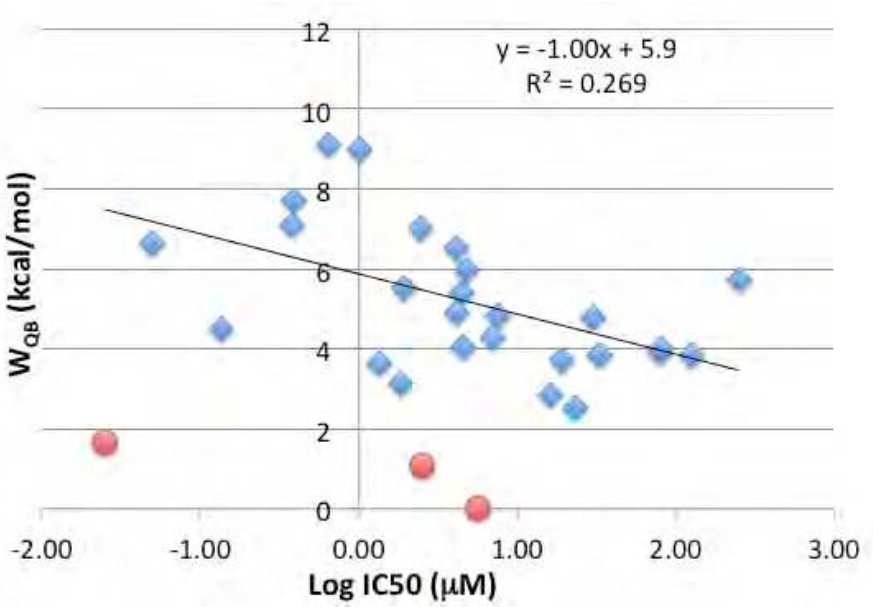

Supplementary Figure 6

ROC curves (left) and semilog-ROC curves (right) of the retrospective virtual screening experiments on CDK2 (top), AA2R (middle) and Trypsin (bottom). The grey line indicates the baseline (random selection). For CDK2, the results corresponding to 2, 8 and 22 DUck runs are reported. For AA2R, the results corresponding to 2, and 8 DUck runs are reported. For Trypsin, only 2 DUck runs were executed. AUC values are inset in the plots.

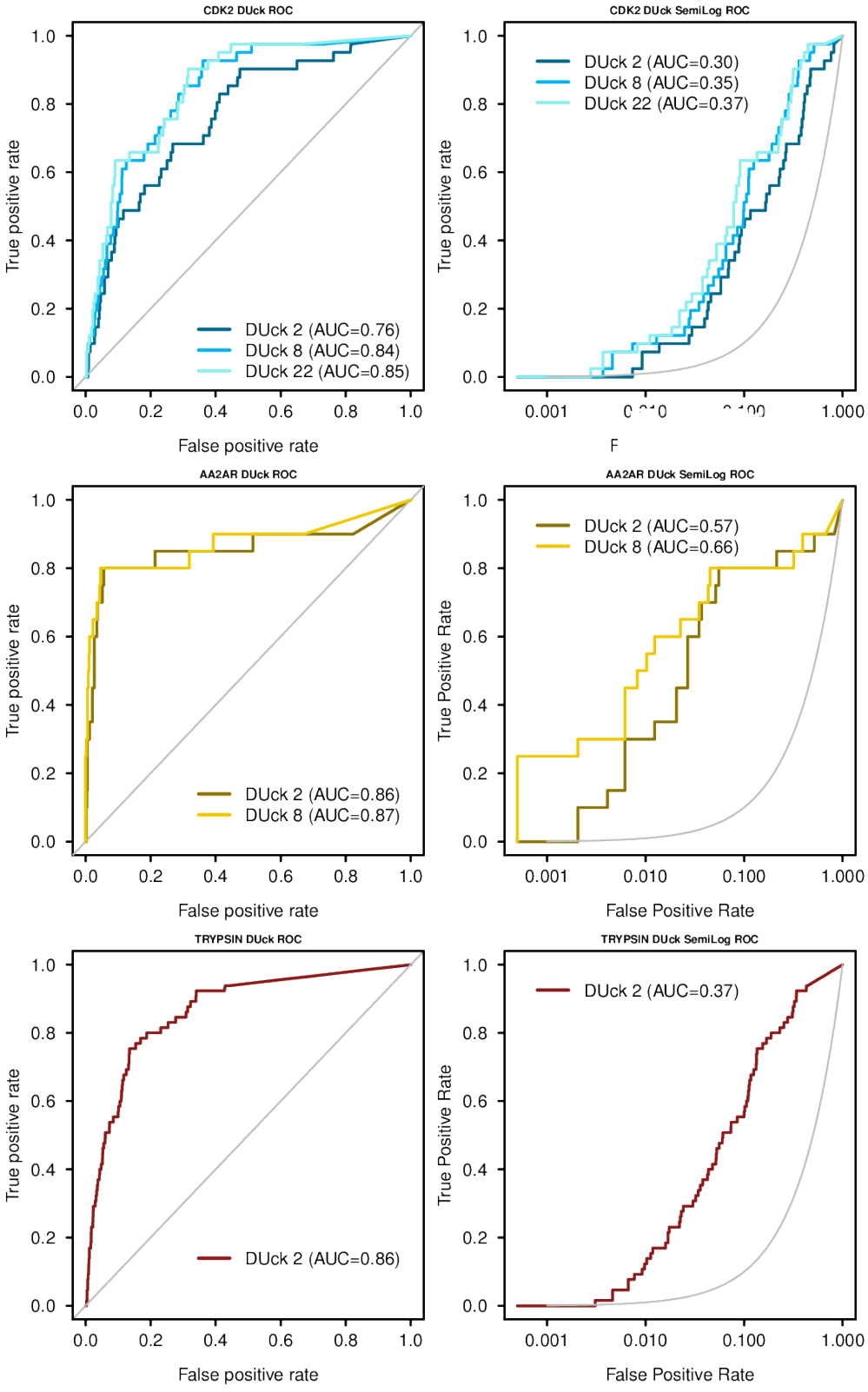

Supplementary Figure 7

Docking (rDock) score vs. W_{QB} values for active (red) and inactive compounds (black or gray) in the retrospective virtual screening datasets for CDK2 (top), AA2AR (middle)and Trypsin (bottom). The side panels show the distribution of active (red) and inactive (black) compounds for each individual method (docking to the left, DUck at the bottom). Gray points (central panel) and gray line (inferior panel) represent the decoys with a docking score within the top 25%. The orange square highlights the area corresponding to top 25% docking score and top 25% W_{QB} values, where optimal enrichment factors (EF) are achieved.

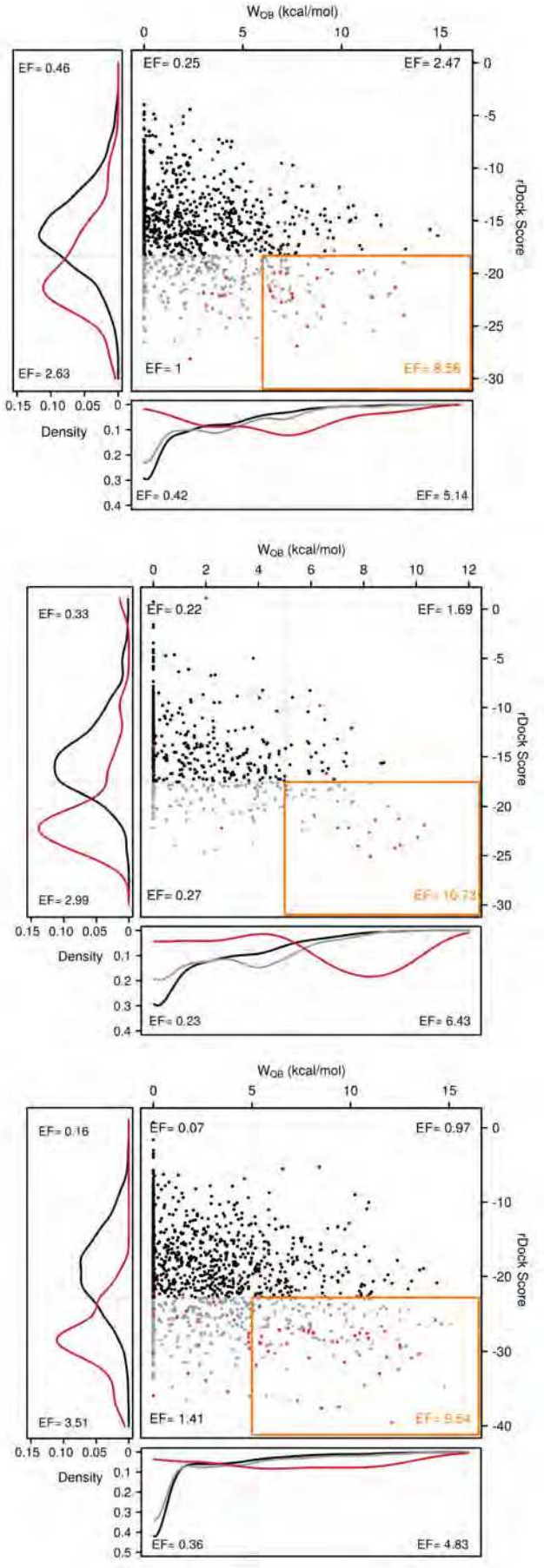

Supplementary Figure 8

Docking score vs. W_{QB} obtained for two different programs on the CDK2 test set. Each molecule was docked with rDock (top) or Glide (bottom) and the binding mode generated by each program was used as starting geometry for DUck simulations. In both cases, docking scores are orthogonal to W_{QB} and a high proportion of good scorers have very low W_{QB} values. The intersection between methods defines a subset highly enriched in active molecules. Two intersecting levels are presented per program:top25% docking+ top 25% DUck (left);and top25% docking + top 12% DUck (right).

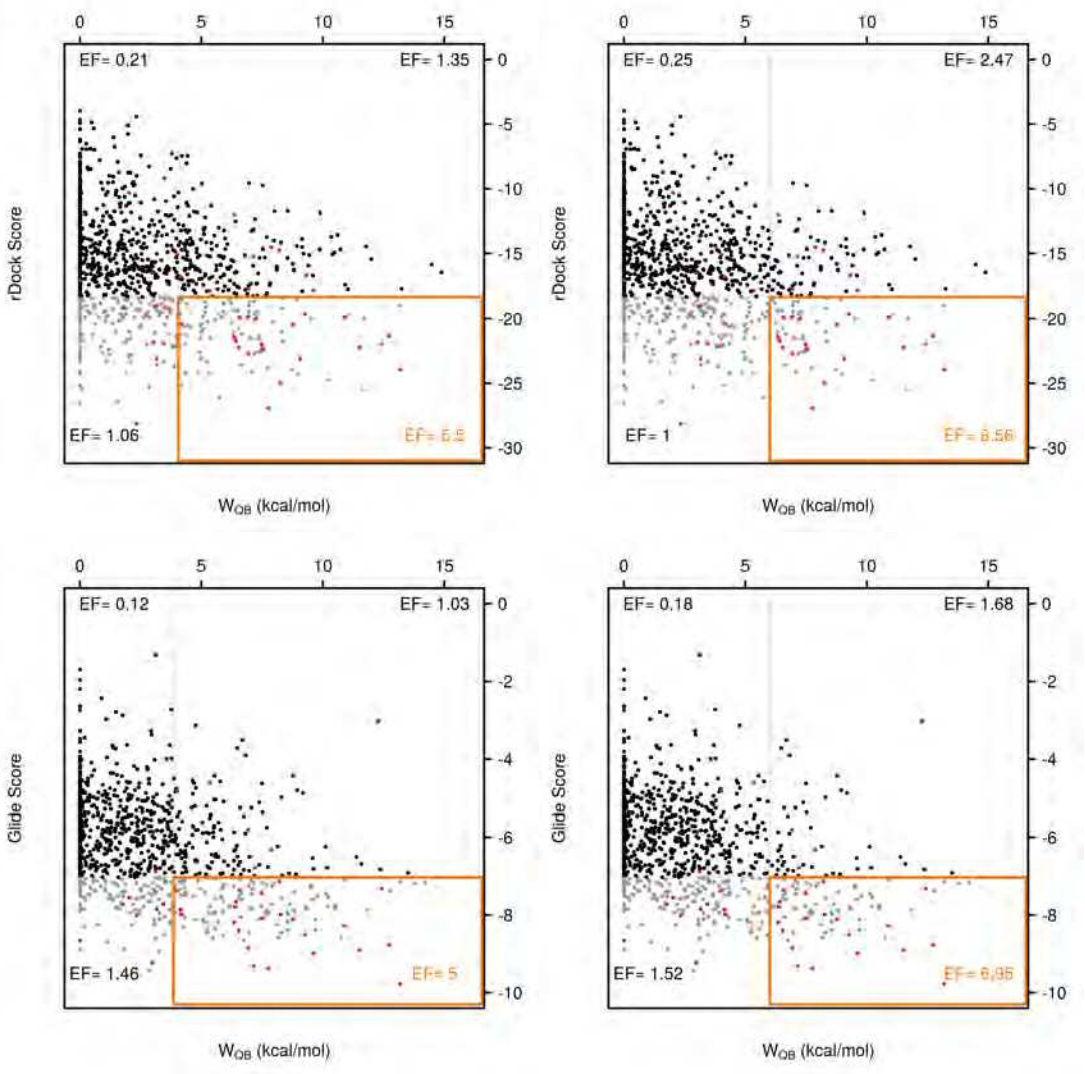

Supplementary Figure 9

MMPBSA and MMGBSA-calculated ΔG_{bind} vs. W_{QB} on the CDK2 test set. The rDock-generated binding mode was used as starting point for molecular dynamics simulations, which where then processed to obtain MMPBSA and MMGBSA binding free energies. In both cases, the calculated ΔG_{bind} values are orthogonal to W_{QB} and a high proportion of good MM(PB/GB)SA scorers have very low W_{QB} values. The intersection between methods defines a subset highly enriched in active molecules. Two intersecting levels are presented per method: top25% MM(PB/GB)SA + top 25% DUck (left); and top25% MM(PB/GB)SA + top 12% DUck (right).

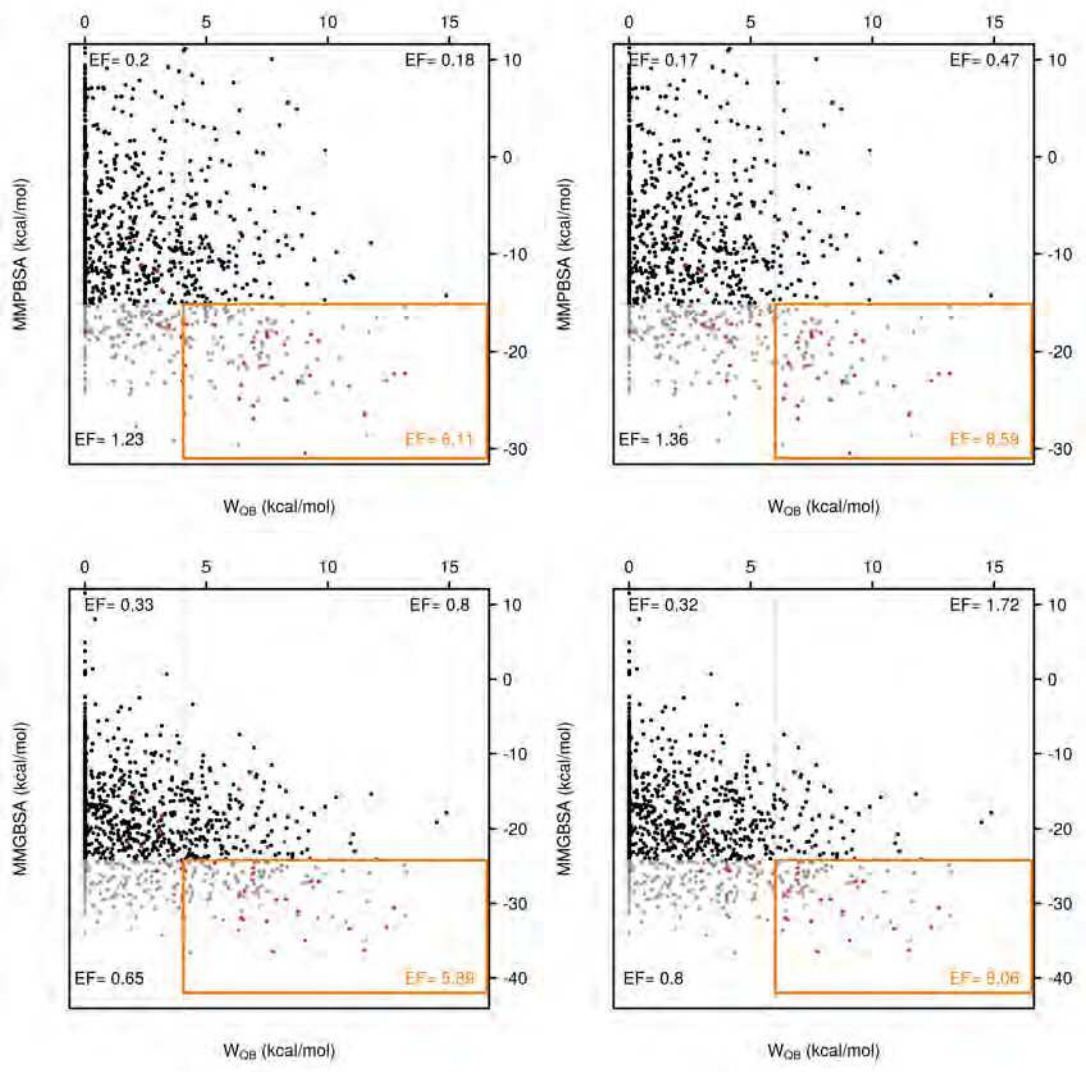

Supplementary Figure 10

Filtering by W_{QB} increases performance even after consensus scoring (CDK2 test set). The left panels show a scatter plot of rDock score vs. Glide score (top) and rDock score vs. MMPBSA-calculated ΔG_{bind} (bottom). Molecules ranked in the top 25% by both methods (highlighted area) are then binned according to their W_{QB} (right panels, also shown in the main text). Filtering by W_{QB} would increase the enrichment factor in a cut-off dependent manner.

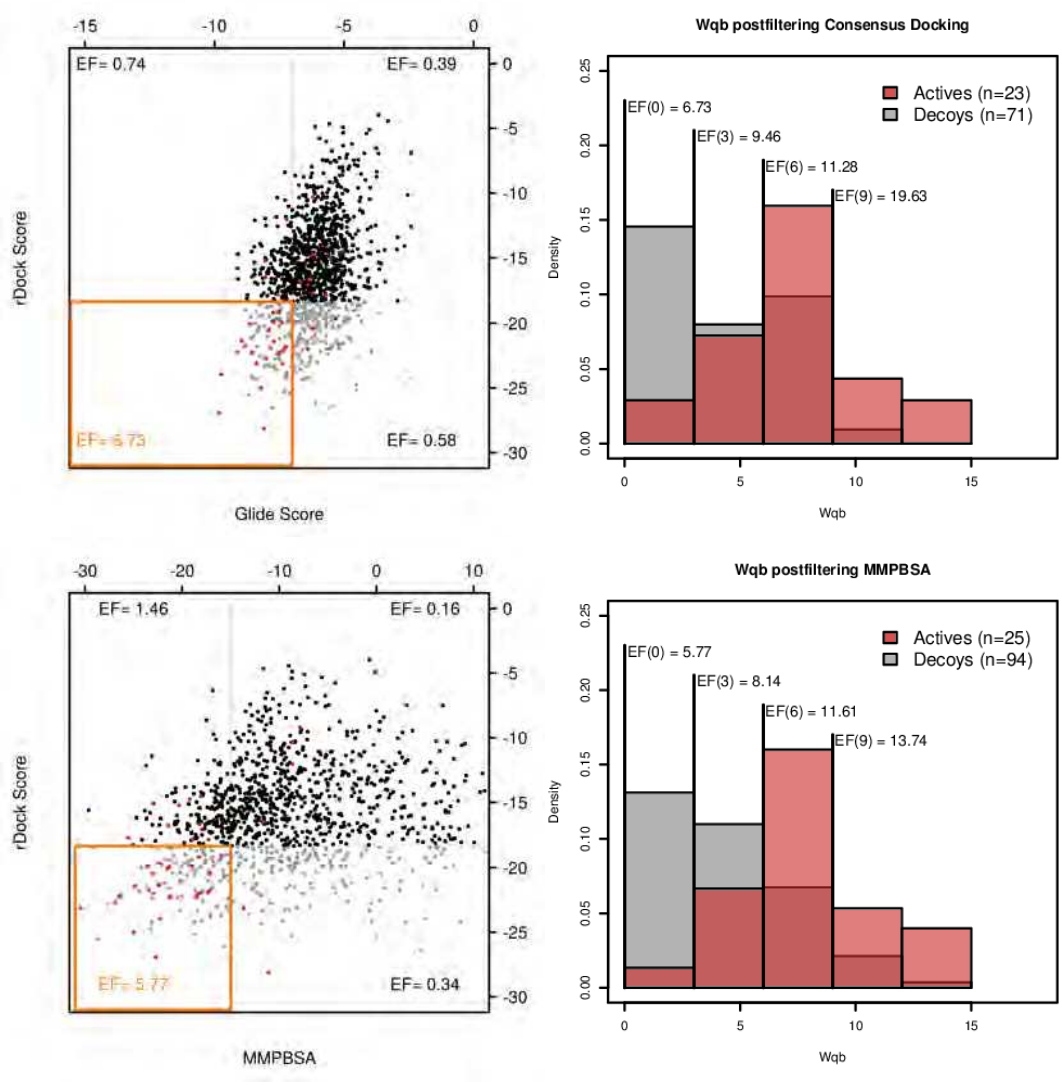

Supplementary Figure 11

Percentage of active molecules in the top 21 (out of 47 compounds tested) as a function of the number of DUck runs. At the screening stage we carried out 100 DUck simulations per ligand, obtaining a hit rate of 38%. Retrospectively, we took 50 random combinations of N={2,4,6,8,10,20,50} DUck runs and calculated the hit rates that would have been obtained. Averages are represented as filled circles and labeled with their actual values. The bars span from the maximum to the minimum values.

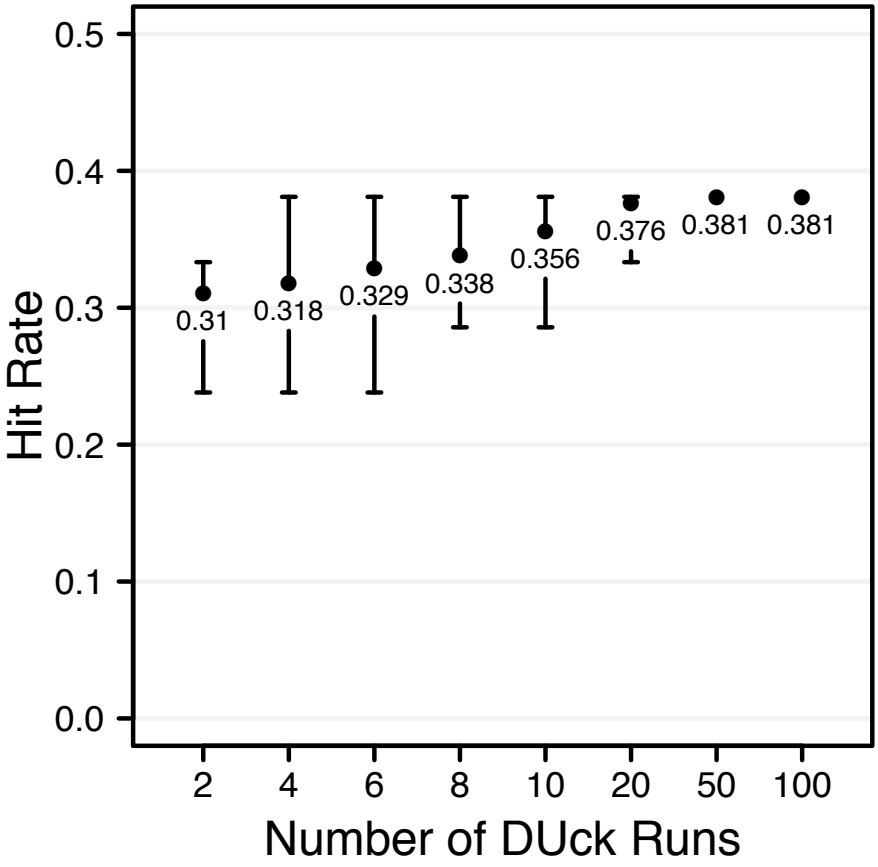

Supplementary Figure 12

Chemical structure of the tested compounds. Duck Class refers to strong, medium and weak binders (1, 2 & 3, respectively). NMR Class 1 are true binders. The rest are considered inactive. The real numbers correspond to rDock score (left) and W_{QB} (right).

DUck Class: 1 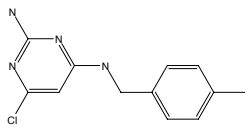 **NMR Class:** 1 -24.9700 9.1000 ID: 1	**DUck Class:** 1 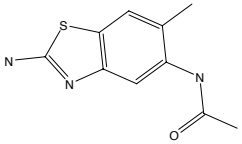 **NMR Class:** 1 -25.0300 8.2000 ID: 2	**DUck Class:** 1 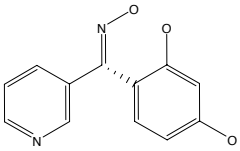 **NMR Class:** 1 -26.6200 11.3000 ID: 3	**DUck Class:** 1 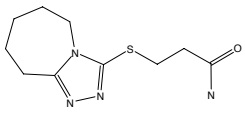 **NMR Class:** 1 -26.4500 7.4000 ID: 4
DUck Class: 1 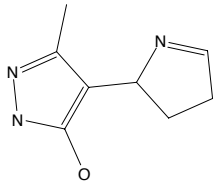 **NMR Class:** 1 -23.7700 8.2000 ID: 5	**DUck Class:** 1 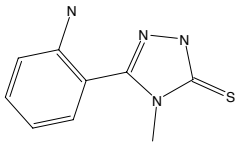 **NMR Class:** 1 -23.2600 9.5000 ID: 6	**DUck Class:** 1 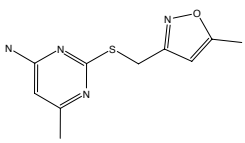 **NMR Class:** 1 -25.4500 7.8000 ID: 7	**DUck Class:** 1 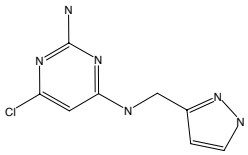 **NMR Class:** 1 -25.3500 7.0000 ID: 8
DUck Class: 1 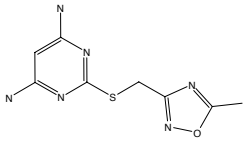 **NMR Class:** 2 -28.0400 7.3000 ID: 9	**DUck Class:** 1 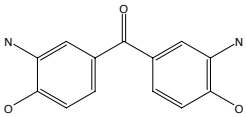 **NMR Class:** 2 -27.1200 6.4000 ID: 10	**DUck Class:** 1 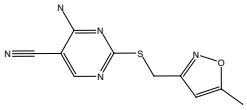 **NMR Class:** 2 -26.1400 9.8000 ID: 11	**DUck Class:** 1 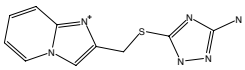 **NMR Class:** 3 -25.4000 7.0000 ID: 12
DUck Class: 1 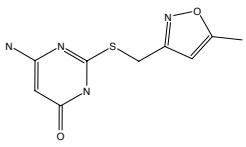 **NMR Class:** 3 -25.0100 6.4000 ID: 13	**DUck Class:** 1 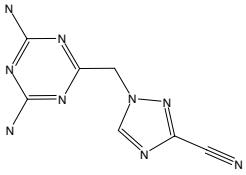 **NMR Class:** nb -26.0000 6.5000 ID: 14	**DUck Class:** 1 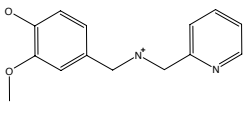 **NMR Class:** nb -25.9100 6.7000 ID: 15	**DUck Class:** 1 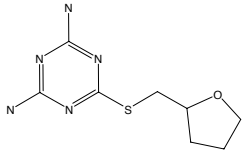 **NMR Class:** nb -24.7300 6.5000 ID: 16
DUck Class: 1 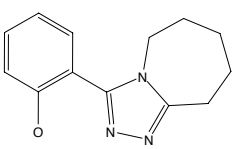 **NMR Class:** nb -24.4600 10.3000 ID: 17	**DUck Class:** 1 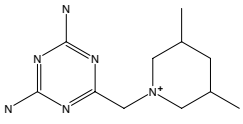 **NMR Class:** nb -28.4400 7.2000 ID: 18	**DUck Class:** 1 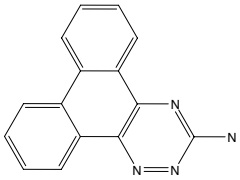 **NMR Class:** nb -25.9200 9.2000 ID: 19	**DUck Class:** 1 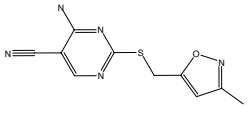 **NMR Class:** nc -26.3400 7.3000 ID: 20

Supplementary Figure 12 (cont)

DUck Class: 1 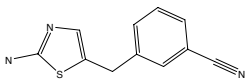 **NMR Class:** r -24.0100 8.0000 ID: 21	**DUck Class:** 2 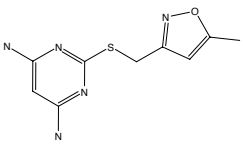 **NMR Class:** 1 -28.2700 5.6000 ID: 22	**DUck Class:** 2 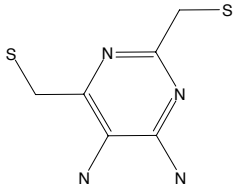 **NMR Class:** 2 -26.8600 4.2000 ID: 23	**DUck Class:** 2 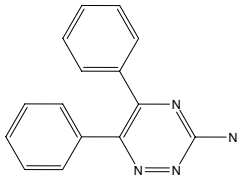 **NMR Class:** 2 -25.3300 3.6000 ID: 24
DUck Class: 2 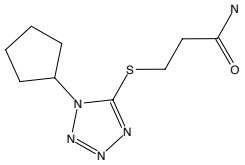 **NMR Class:** 2 -25.3200 3.9000 ID: 25	**DUck Class:** 2 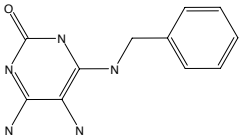 **NMR Class:** 3 -25.0900 5.5000 ID: 26	**DUck Class:** 2 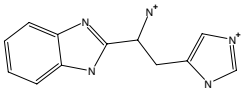 **NMR Class:** 3 -27.3400 3.5000 ID: 27	**DUck Class:** 2 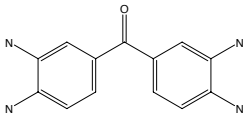 **NMR Class:** 3 -27.5500 3.2000 ID: 28
DUck Class: 2 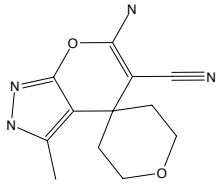 **NMR Class:** nb -25.4600 4.7000 ID: 29	**DUck Class:** 2 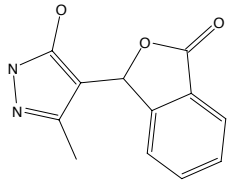 **NMR Class:** nb -25.0900 5.5000 ID: 30	**DUck Class:** 2 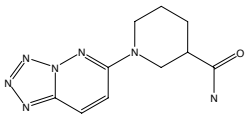 **NMR Class:** nb -26.7600 4.4000 ID: 31	**DUck Class:** 2 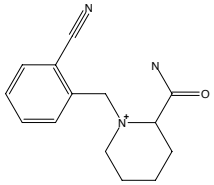 **NMR Class:** nb -26.4700 3.1000 ID: 32
DUck Class: 2 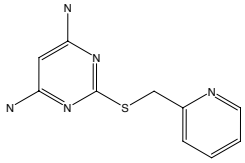 **NMR Class:** nb -25.1000 4.9000 ID: 33	**DUck Class:** 2 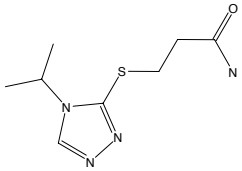 **NMR Class:** nb -24.8300 4.8000 ID: 34	**DUck Class:** 2 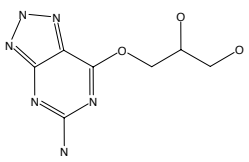 **NMR Class:** nb -24.3200 4.4000 ID: 35	**DUck Class:** 2 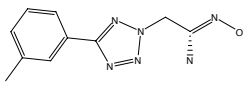 **NMR Class:** nb -26.8200 3.0000 ID: 36
DUck Class: 3 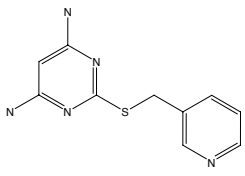 **NMR Class:** 2 -27.9100 0.8000 ID: 37	**DUck Class:** 3 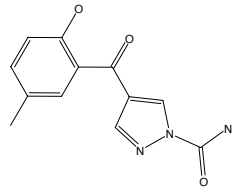 **NMR Class:** 2 -26.2500 1.4000 ID: 38	**DUck Class:** 3 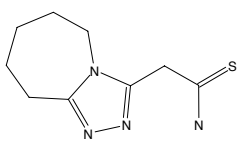 **NMR Class:** 2 -25.4700 0.5000 ID: 39	**DUck Class:** 3 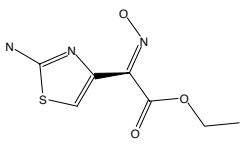 **NMR Class:** 3 -25.3700 1.0000 ID: 40

Supplementary Figure 12 (cont)

DUck Class: 3 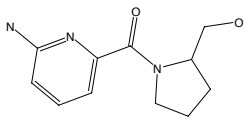 **NMR Class:** nb -26.4800 2.3000 ID: 41	**DUck Class:** 3 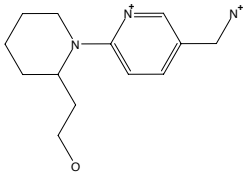 **NMR Class:** nb -25.7700 2.5000 ID: 42	**DUck Class:** 3 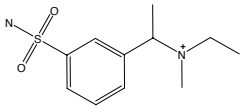 **NMR Class:** nb -24.9900 0.0000 ID: 43	**DUck Class:** 3 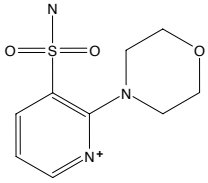 **NMR Class:** nb -24.9700 0.0000 ID: 44
DUck Class: 3 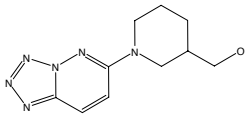 **NMR Class:** nb -24.9100 0.0000 ID: 45	**DUck Class:** 3 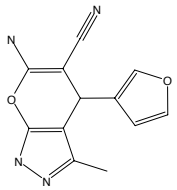 **NMR Class:** nb -23.2300 2.0000 ID: 46	**DUck Class:** 3 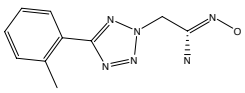 **NMR Class:** nb -26.1100 1.7000 ID: 47	

Supplementary Figure 13

Crystal structure of Hsp90 in complex with compounds **1** (top), **2** (middle) and **3** (bottom). The 2fofc electron density maps are displayed at the 1.0 Sigma level (Carve = 1.7).

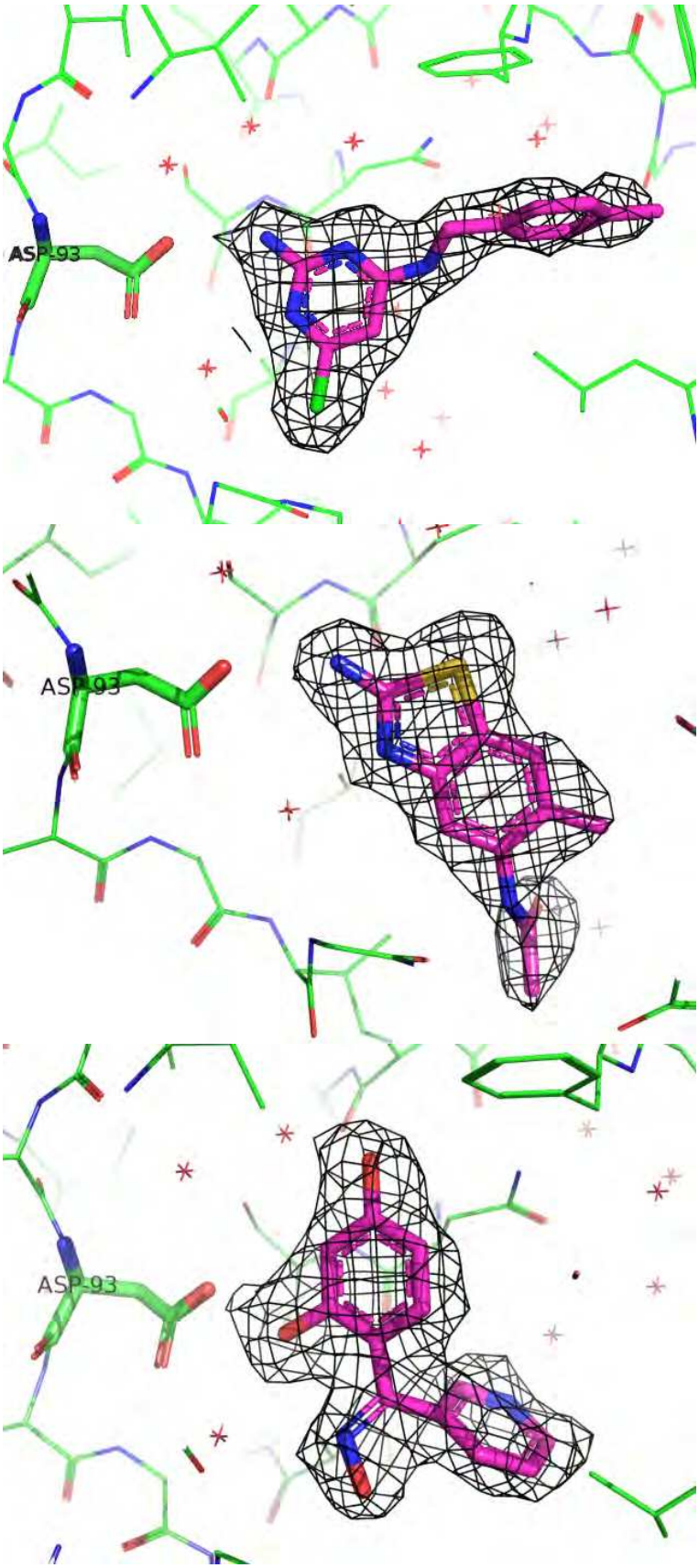

Supplementary Figure 14

Predicted binding modes for compounds **4**, **5** and **6** (from left to right).

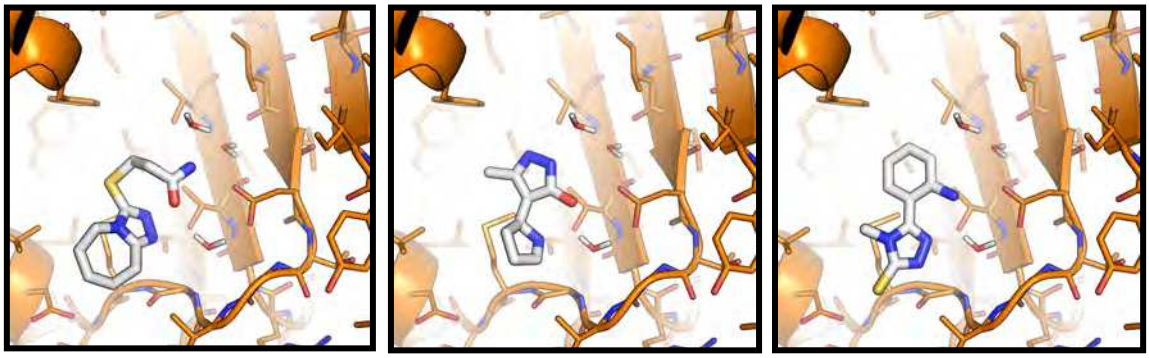

Supplementary Figure 15

Dependence of the results on the size of the receptor. W_{QB} values of CDK2 ligands were calculated using the whole protein as receptor and plotted against the results obtained with a truncated system (top). W_{QB} values obtained with the truncated system represent a lower bound to those obtained with the full system. This indicates that when the whole system is included, W_{QB} may not reflect the contribution of the interaction under investigation. Potentially, this may give rise to false positives. Noteworthy, the virtual screening results are comparable to those obtained with the truncated system (bottom; compare with Supplementary Figure 8).

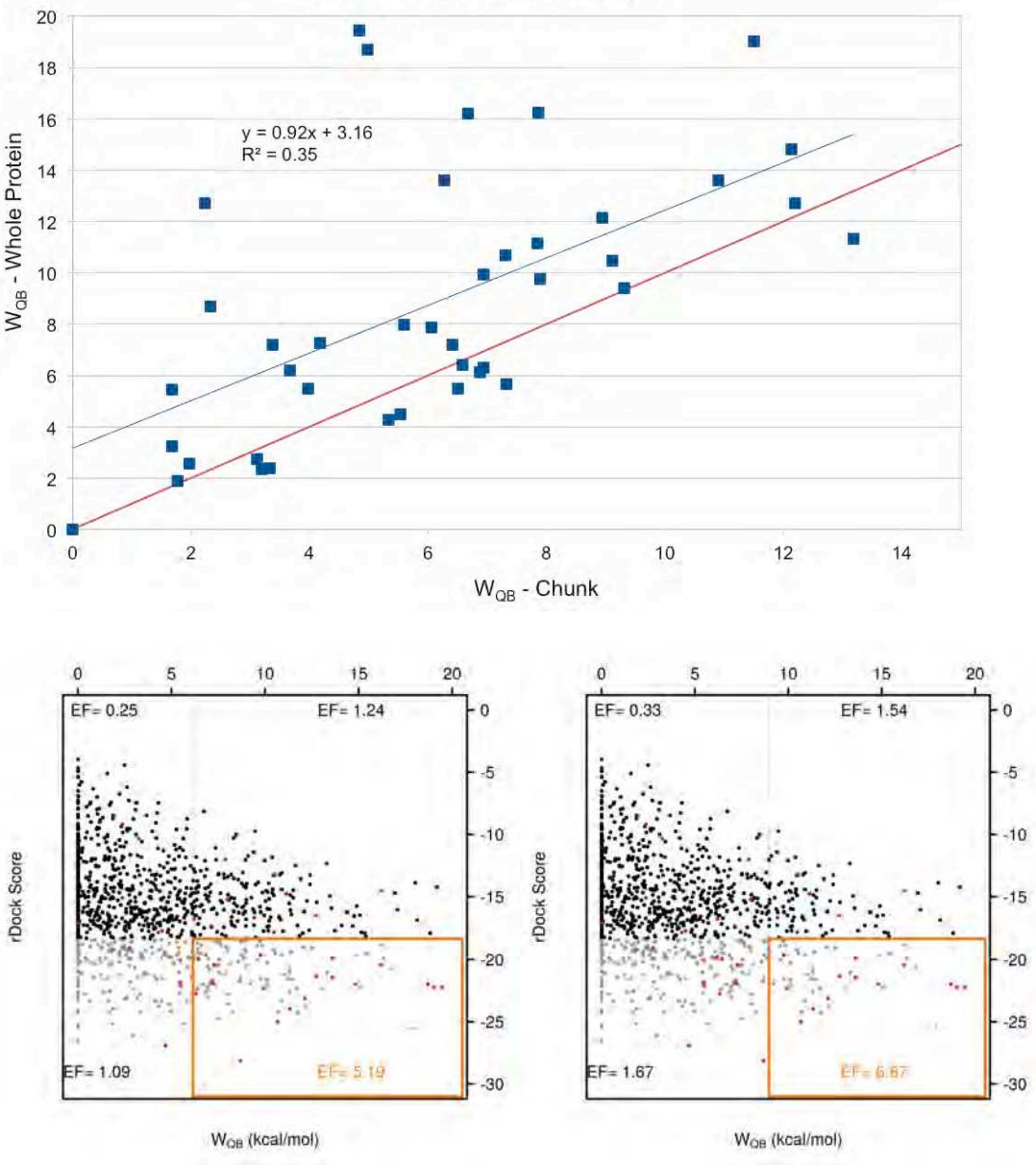

Supplementary Figure 16

Dependence of the results on the steering velocity. Two different velocities are compared: 5 Å·ns^{-1} (used through this work) and 1.25 Å·ns^{-1}. Slower velocities mean more sampling and, potentially, lower W_{QB} values. The high correlation (r^2=0.94) indicates that the standard conditions (v=5 Å·ns^{-1}) produce converged results.

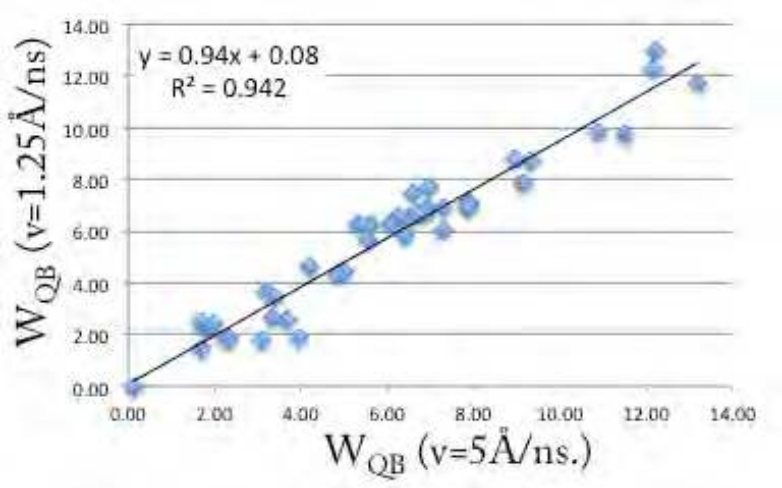

Supplementary Figure 17

Dependence of the results on the choice of reaction coordinate. W_{QB} values obtained using two different atoms of reference in the hinge region of CDK2 are highly correlated (top) and afford similar enrichment factors in retrospective virtual screening (bottom; compare with Supplementary Figure 8). The atoms used as reference (Leu83:N in the x-axis and Leu83:O in the y-axis) are part of the hinge and located in close proximity (3Å). Most ligands form a hydrogen bond with both atoms at the same time. Points in red represent ligands that only form a hydrogen bond with Leu83:N.

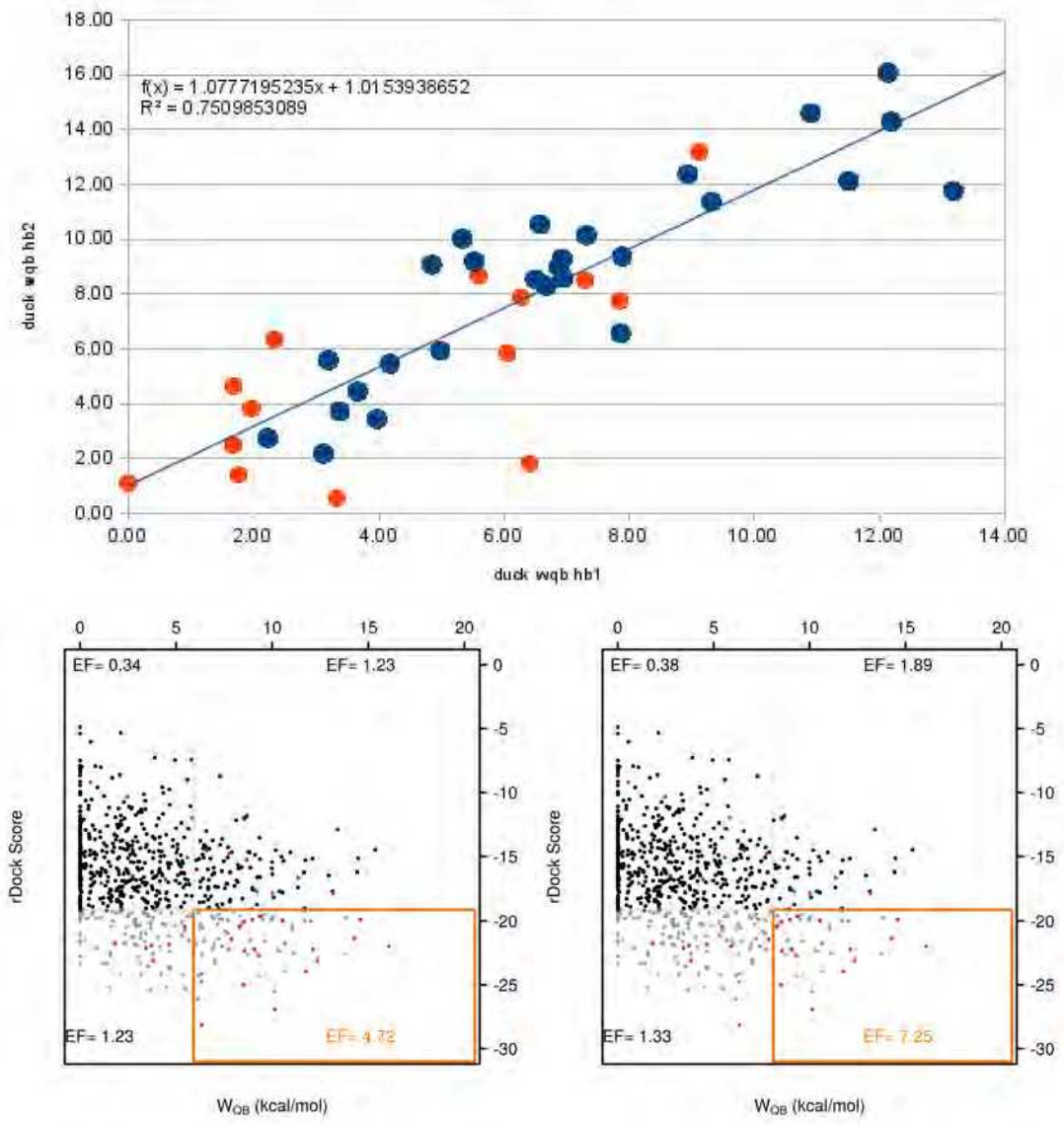

Supplementary Figure 18

W_{QB} of CDK2 ligands pulling the amine of Lys33 and comparison with W_{QB} values obtained for the hinge region (in kcal/mol). Only those ligands capable of forming a hydrogen bond with NZ of Lys33 have been considered. It should be noted that this part of the active site presents large conformational diversity between structures. In consequence, the DUck results may be less reliable than for the hinge region.

PDB Code	W_{QB} (O Leu83)	W_{QB} (Nζ Lys33)
1OIQ	4.48	5.18
3BHT	6.59	9.65
3BHV	6.94	0.00
3EJ1	5.77	2.06
3FZ1	0.12	10.50
3QTQ	6.66	5.56
3QTW	9.76	5.91
3TIY	3.47	0.00

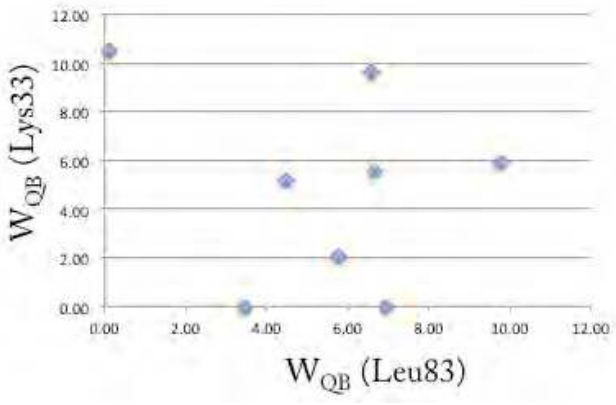

Supplementary Figure 19

Proposed protocol for DUck-based virtual screening and comparison with MMPBSA. The smaller size of the system speeds up calculations by a factor or 5 (Supplementary Table 2), also permitting shorter equilibration times. Each ligand undergoes equilibration and at least two SMDs (45 GPU minutes). Molecules with W_{QB} above a given threshold (e.g. t=6 kcal/mol) would then proceed to N cycles of unbiased MD + SMD simulations (42 GPU minutes per cycle). A similar protocol for MMPBSA would require at least 2 GPU hours of equilibration followed by N cycles of 1ns MD simulation and MMPBSA calculation of representative snapshots (1 GPU hour + 20 CPU minutes per cycle).

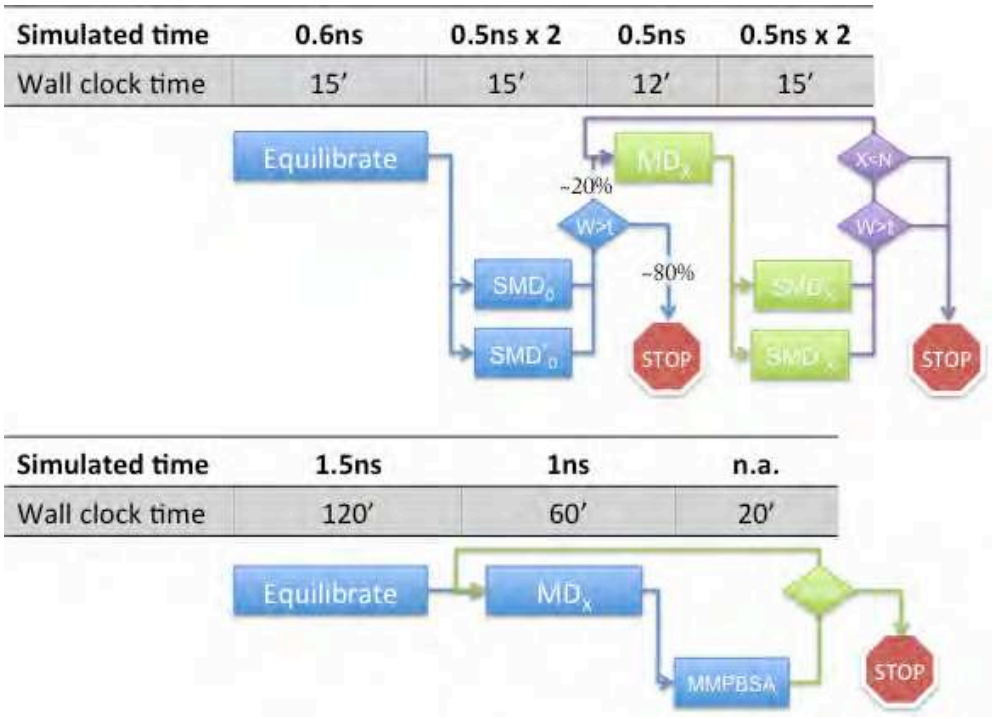

Supplementary Figure 20

CDK2 test set: correlation between LogIC50 and W_{QB} is not caused by Molecular Weight. The correlation between W_{QB} and MW (r^2=0.07) is lower than the correlation between W_{QB} and LogIC50 (r^2=0.23) or between LogIC50 and MW (r^2=0.36). Red points (discussed in Supplementary Figure 2) are excluded from all correlations.

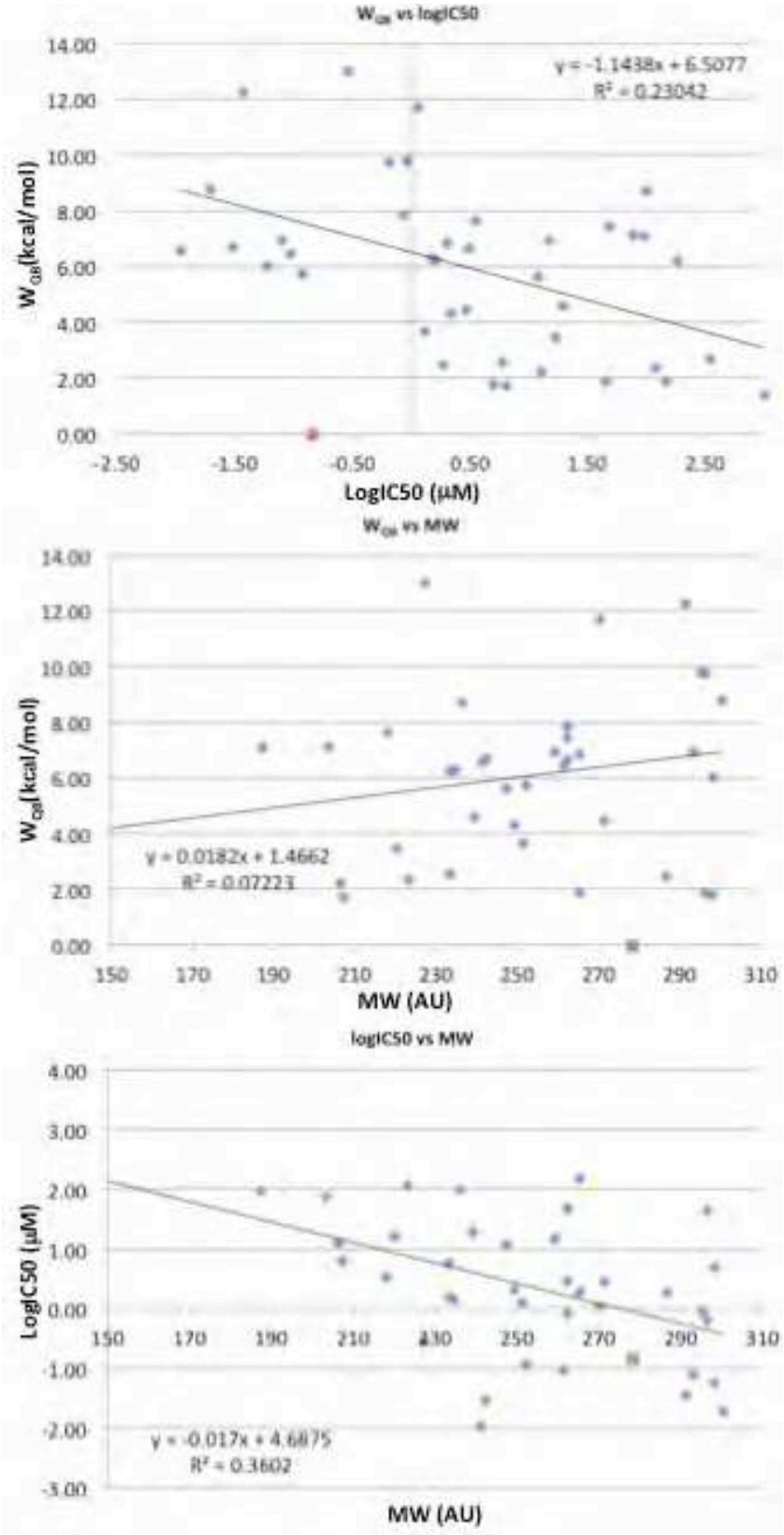

Supplementary Figure 21

BRD4 test set: correlation between LogIC50 and W_{QB} is not caused by Molecular Weight. The correlation between W_{QB} and MW (r^2=0.17) is lower than the correlation between W_{QB} and logIC50 (r^2=0.26) or between LogIC50 and MW (r^2=0.43). Red points (discussed in Supplementary Figure 5) are excluded from all correlations.

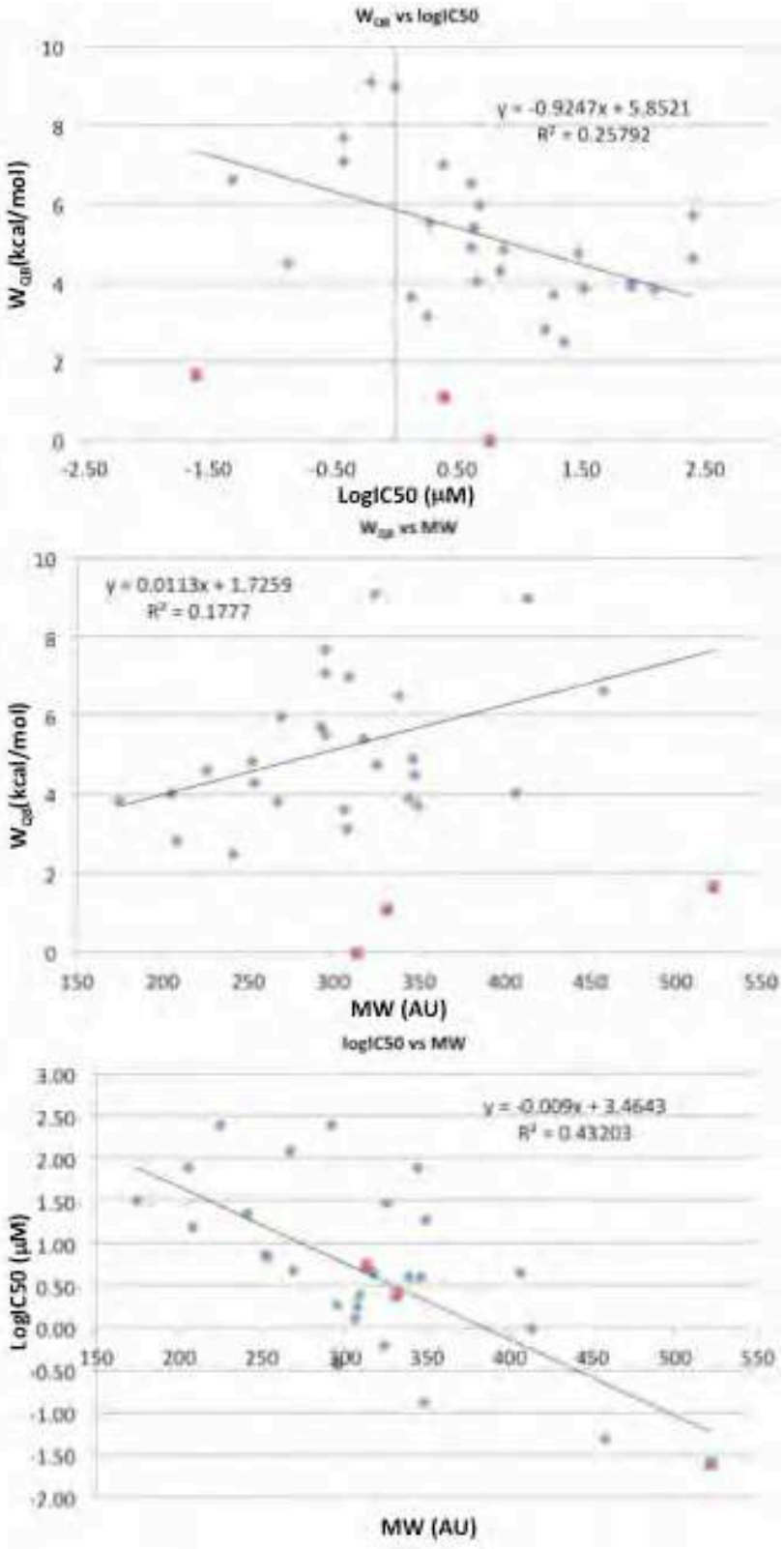

CDK2 AA2AR

Supplementary Figure 22

ROC curves comparison of DUck (in standalone mode) with unbiased docking with Glide and rDock for the three test systems: CDK2, AA2AR and Trypsin.

TRYPSIN

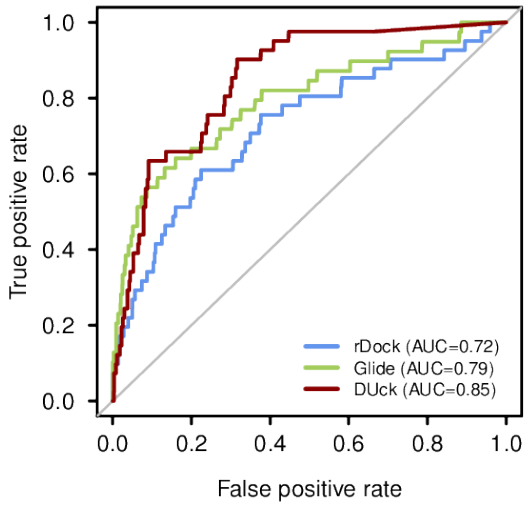

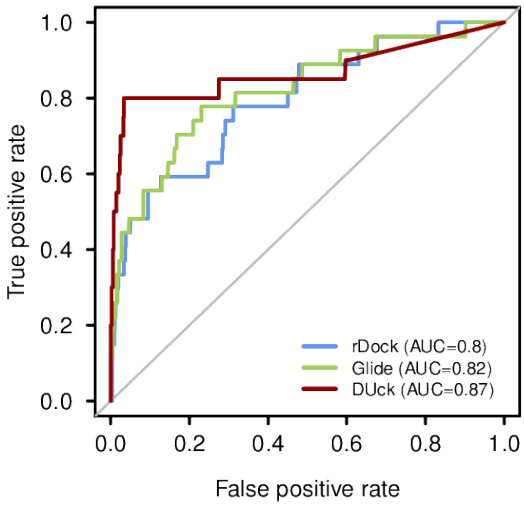

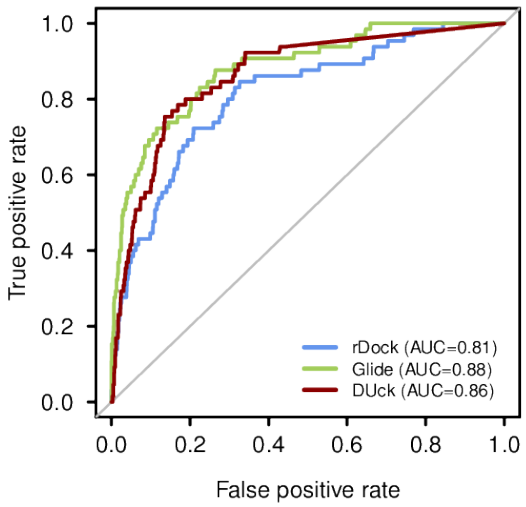

CDK2

AA2AR

Supplementary Figure 23

ROC curves comparison of DUck (in standalone mode) with pharmacophore-guided docking with Glide and rDock for the three test systems: CDK2, AA2AR and Trypsin.

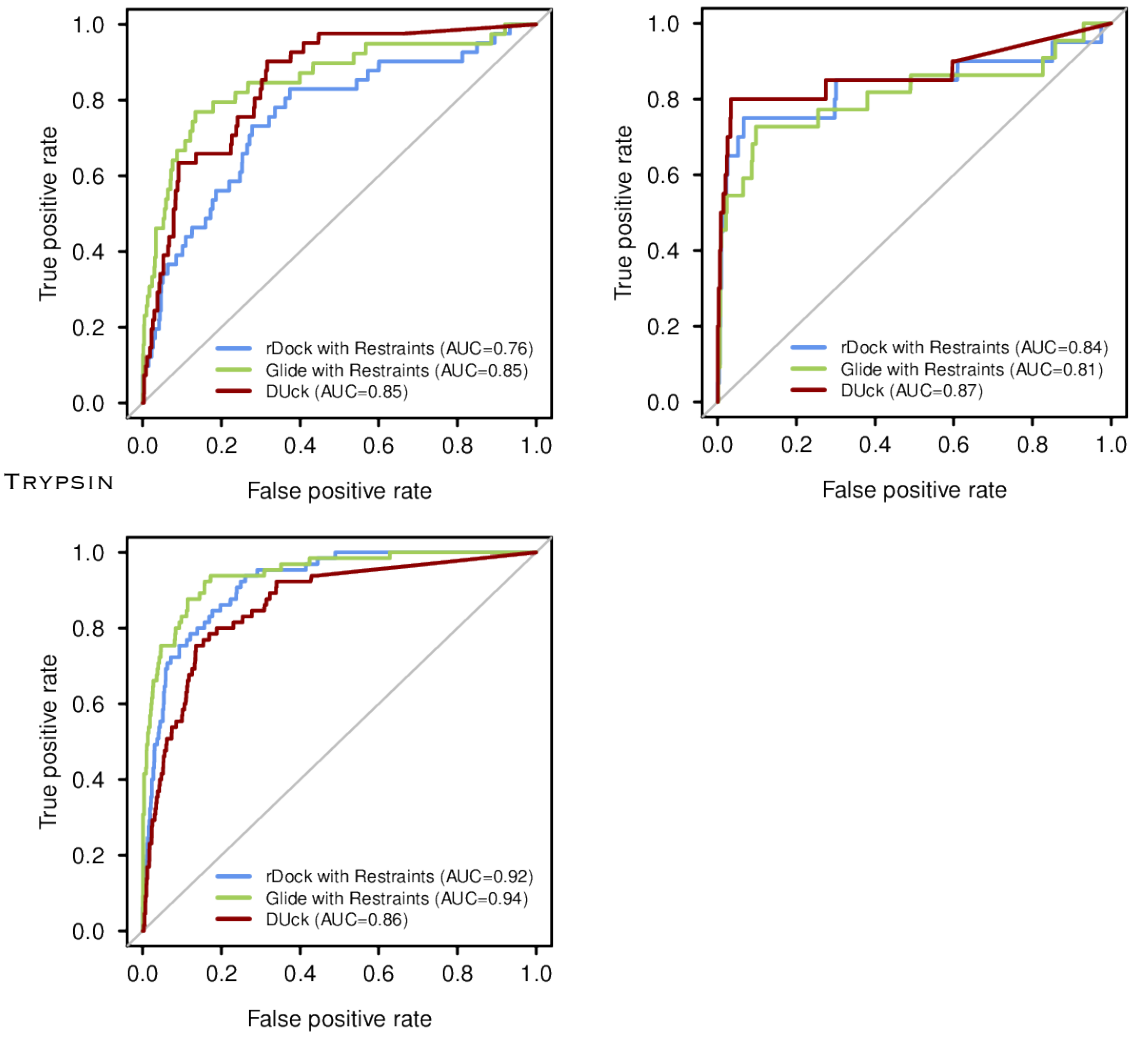

Supplementary Figure 24

DUck postfiltering improves early enrichment. Semilogarithmic ROC curves for the retrospective virtual screening of CDK2, obtained with the best-performing program for this test set (Glide),alone or in combination with three different postfiltering methods: DUck (left); MMPBSA (middle) and rDock (right). Ligands were initially ranked according to Glide's score. Then, moved to the back of the list if they were not in the top 12% of the rescoring method. This shows that the Glide-DUck combination is superior to Glide alone. For this test set the effect is most prominent in the top 1% to 5% of the library. Glide-MMPBSA combination is provided for comparison and affords very similar results. The Glide-rDock combination does not improve early enrichment.

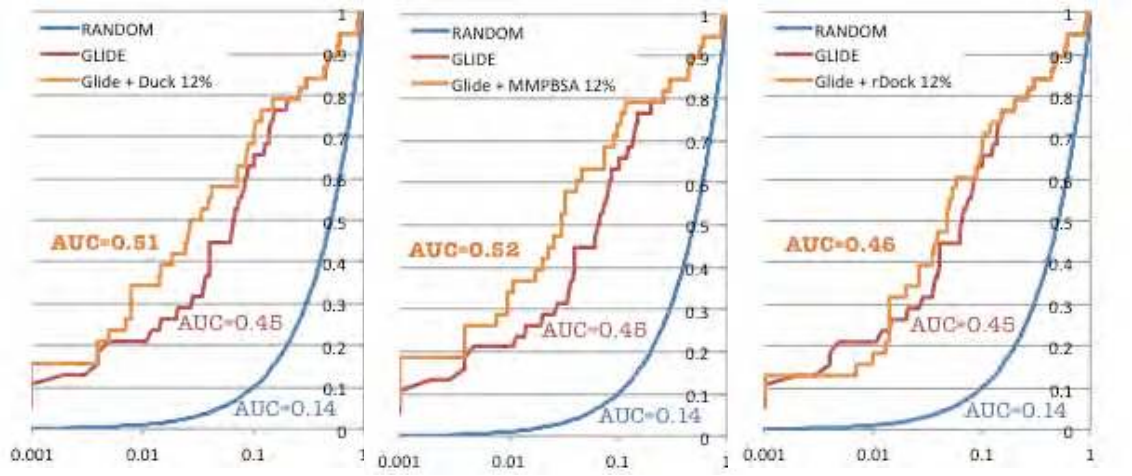

Supplementary Figure 25

ROC curves comparison of DUck (in standalone mode) with MMPBSA and MMGBSA for CDK2

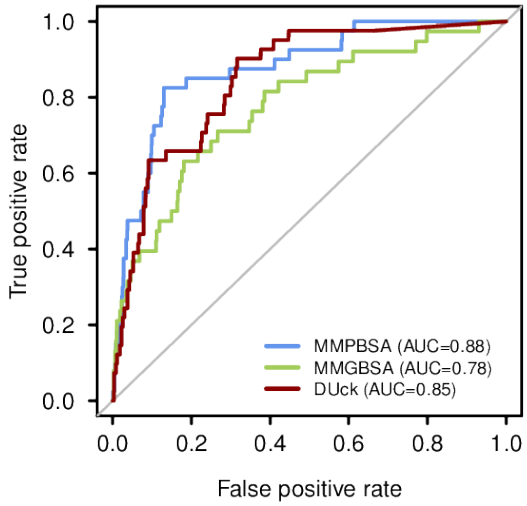

Supplementary Figure 26

Examples of typical sensorgrams (left column) and steady state plots (right column) for the binding of the fragment hits to Hsp90. Fragments were tested in a 2-fold dilution series starting at 500uM or 250uM concentrations. Steady state values were calculated 4seconds before the injection stopped and plotted against the concentration. The K_D value was calculated by fitting the data to a steady state affinity model (Biacore T200 evaluation software GE Healthcare)

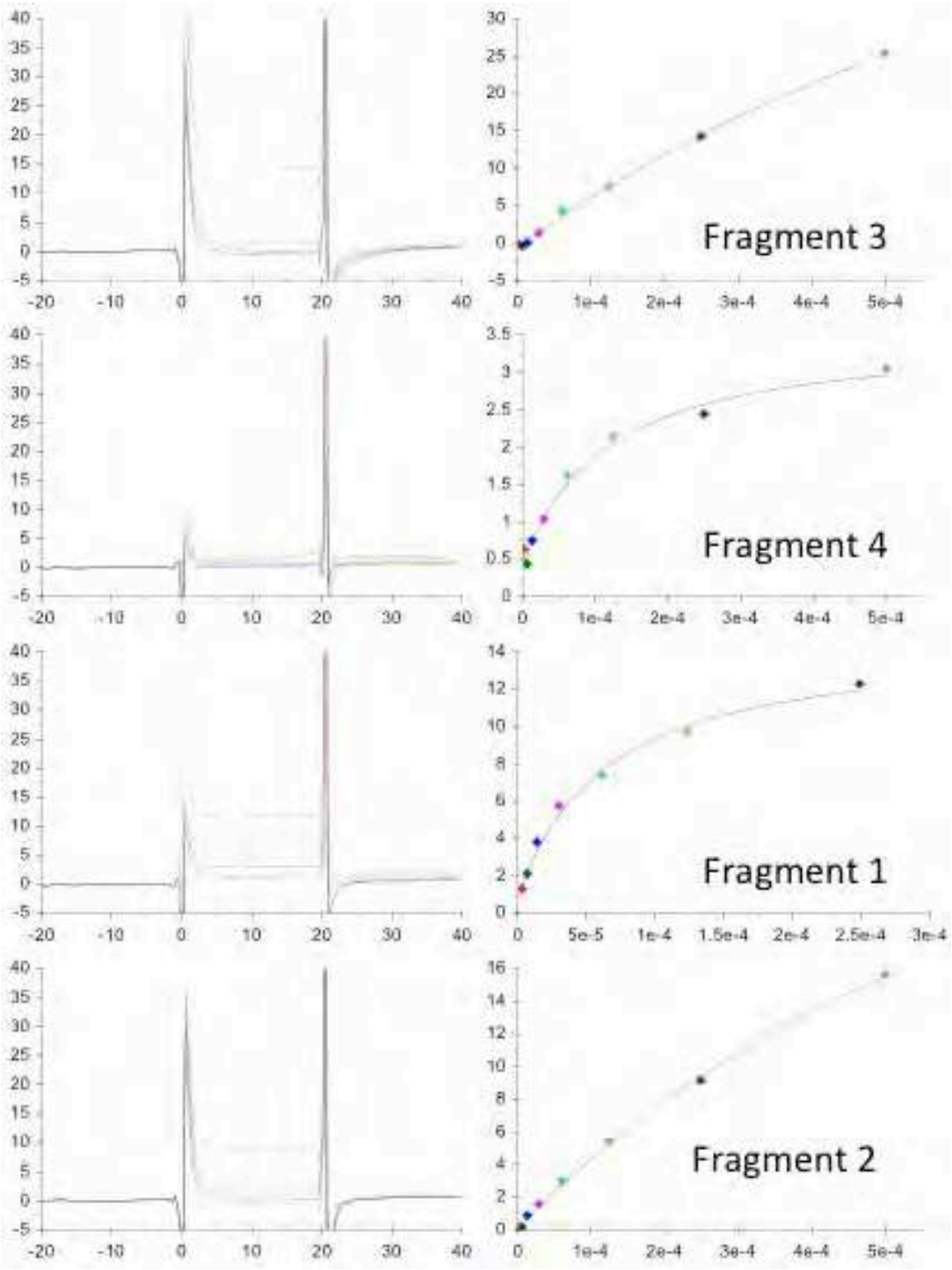

SUPPLEMENTARY TABLES

Supplementary Table 1

Chemical structures and summary of results for the 9 Hsp90 NMR Class 1 hits.

ID	Structure	MW	Docking		DUck		Xray	SPR Kd (mM)	PDB Sim[b]	ChEMBL Sim[b]
			Score	*Rank*[a]	W_{QB}	*Rank*[a]				
1	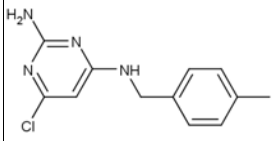	248,72	-24,97	*79*	9,1	*10*	Yes	77	2XDX (0.37)	CHEMBL 1340447 (0.44)
2	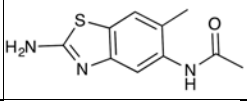	221,29	-25,03	*73*	8,2	*11*	Yes	320	2WI6 (0.29)	CHEMBL 1536318 (0.54)
3	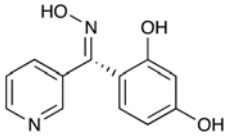	230,22	-26,62	*19*	11,3	*1*	Yes	700	4EFU (0.32)	CHEMBL 1458840 (0.51)
4	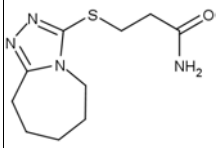	240,33	-26,45	*22*	7,4	*16*	-	730	3WHA (0.29)	CHEMBL 1542436 (0.37)
5	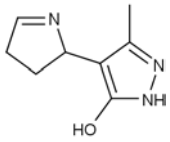	165,20	-23,77	*128*	8,1	*12*	-	-	4EFT (0.27)	CHEMBL 1313412 (0.28)
6	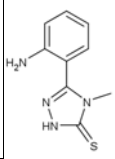	206,27	-23,26	*138*	9,5	*5*	-	-	3HHU (0.42)	CHEMBL 2103879 (0.42)
7	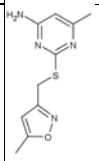	236,30	-25,45	*51*	7,8	*15*	-	-	3B24 (0.31)	CHEMBL 1375884 (0.36)
8	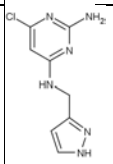	224,66	-25,35	*58*	7,0	*22*	-	-	2XDX (0.35)	CHEMBL 1383799 (0.37)
22	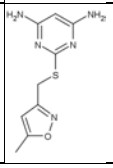	237,29	-28,27	*2*	5,6	*33*	-	-	3O0I (0.27)	CHEMBL 1834092 (0.33)

[a] Position within the list of 149 molecules that were evaluated with DUck. [b]Hsp90 structure in the PDB or compound with Hsp90 activity in ChEMBL (as of 23/03/2016) with the closest similarity to the fragment hit. Similarity (values in parentheses) was calculated with Open Babel using the FP2 fingerprint.[14]

Supplementary Table 2

Number of atoms of the investigated systems. On average, using a protein chunk with explicit solvation produces a system 20% in size relative to the whole protein. As computational times scale linearly with the number of particles, this represents a 5-fold gain in efficiency.

Number of Atoms

	Full System		Protein Chunk for DUck	
System	Protein	Periodic Box[a]	Protein[b]	Periodic Box[a,b]
Hsp90	3291	30387	527 (16,0%)	9415 (31,0%)
Cdk2	4578	46803	345 (7,5%)	9110 (19,5%)
AA2AR	4603	73039	525 (11,4%)	8815 (12,1%)
Trypsin	3231	26721	335 (10,4%)	9696 (36,3%)
Average	3926	44238	433 (11,0%)	9259 (20,9%)

[a] Protein solvated with TIP3 water molecules using Amber's tleap program. In all cases, the periodic system is a truncated octahedral box, the distance parameter is 12.0 and the closeness parameter is 0.65.[b] Values in parentheses are percentage of atoms relative to the full system.

Supplementary Table 3

Detail of the receptor definition used in DUck simulations. Water and residue numbers were taken from the corresponding PDB file.

System	Reference Atom	PDB Code (Chain)	Protein residues included as receptor	Water Molecules
CDK2	LEU 83 NH	1CKP (A)	ILE10 VAL18 LYS20 ALA21 VAL29 VAL30 ALA31 LEU32 VAL64 PHE80 GLU81 PHE82 LEU83 HIS84 GLN85 ASP86 LEU133 LEU134 ILE135 ASN136 ALA144	-
AA2AR	ASN 253 ND2	3EML (A)	LEU167 PHE168 GLU169 VAL172 PRO173 MET174 MET177 VAL178 ASN181 PHE182 TRP246 LEU247 PRO248 LEU249 HIS250 ILE251 ILE252 ASN253 CYS254 PHE255 THR256 PHE257 HIS264 ALA265 PRO266 LEU267 MET270 TYR271 LEU272 ALA273 ILE274	-
Trypsin	ASP189 OD1	2AYW (A)	HIS57 LEU99 ASP102 ASP189 SER190 CYS191 GLN192 GLY193 ASP194 SER195 VAL213 SER214 TRP215 GLY216 SER217 GLY219 CYS220 ALA221A GLN221 LYS224 PRO225 GLY226 VAL227 TYR228 THR229	1017 1096 1098 1101
Hsp90	ASP93 OD2	2YED (A)	GLU47 LEU48 ILE49 SER50 ASN51 SER52 SER53 ASP54 ALA55 LEU56 ASP57 LYS58 ILE78 ILE91 VAL92 ASP93 THR94 GLY95 ILE96 GLY97 MET98 GLY137 PHE138 VAL150 ILE151 THR152 GLY183 THR184 LYS185 VAL186	2043 2045 2049 2105 2107
BRD4	ASN140 ND2	3U5L (A)	TRP81 PRO82 PHE83 GLN84 GLN85 PRO86 VAL87 ASP88 ALA89 LYS91 LEU92 ASN93 LEU94 TYR97 ILE101 PRO104 MET105 THR131 ASN135 CYS136 TYR137 TYR139 ASN140 ASP144 ASP145 ILE146 MET149	-

Supplementary Table 4

Data collection and refinement statistics for Hsp90 in complex with Compounds **1**, **2** and **3**.R_{free} is the R factor calculated using 5% of the reflection data chosen randomly and omitted from the refinement process, whereas R_{cryst} is calculated with the remaining data used in the refinement. Rms bond lengths and angles are the deviations from ideal values; the rms deviation in B factors is calculated between covalently bonded atoms.

Compound	**1**	**2**	**3**
Data collection statistics			
Resolution (Å)	2.20	2.00	2.10
Space group	I222	I222	I222
Cell dimensions (Å)			
a =	66.87	64.96	68.98
b =	90.29	88.41	88.18
c =	98.33	99.06	96.90
No. molecules/asymmetric unit	1	1	1
Solvent content (%)	57.25	54.73	57.41
Measured reflections	66152	66886	62479
Unique reflections	15401	19011	17526
Completeness: Overall / in hrb[a] (%)	99.5 / 98.5	96.7 / 90.9[b]	99.4 / 99.9
Mean I/σI: Overall / in hrb	11.2 / 2.8	11.1 / 1.3	8.33 / 0.95
R_{merge}: Overall / in hrb (%)	0.083 / 0.315	0.048 / 0.412	0.074 / 0.555
Refinement statistics			
R_{free} (%)	24.0	30.8[b]	27.6
R_{cryst} (%)	19.1	22.1	22.4
Rms Deviations:			
Bonds (Å)	0.018	0.019	0.019
Angles (°)	1.920	1.958	2.046
B Factor (Å^2)	4.679	5.536	6.415
PDB Code	5FNC	5FND	5FNF

[a]hrb: highest resolution bin. [b]Diffraction data for this structure was collected from a crystal that did not cryo-freeze correctly therefore the data in some of the resolution bins was of a lesser quality than the equivalent data collected from the other two crystals. This is likely to have impacted the refinement statistics for this structure.

Supplementary Table 5

List of ligands in the CDK2 test set. Ligands highlighted in red are not included in the correlation plotted in Supplementary Figure 2 and Supplementary Figure 25.

PDB	No.Atoms	MW	IC50 (uM)	Log IC50	W_{QB} (kcal/mol)
1E1V	21	247.303	12.00	1.08	5.53
1E1X	22	251.292	1.30	0.11	3.19
1JSV	23	265.293	2.00	0.30	6.93
1JVP	19	233.274	1.60	0.20	5.59
1OIQ	23	271.325	2.90	0.46	4.98
1PF8	21	242.26	0.03	-1.51	6.88
1PXJ	16	206.267	13.00	1.11	1.76
1PXK	19	249.293	2.20	0.34	4.84
1PXM	23	298.365	0.06	-1.22	7.32
1VYW	24	291.355	0.04	-1.43	12.13
1VYZ	19	227.268	0.29	-0.54	12.19
1W0X	25	298.351	5.00	0.70	3.97
1WCC	10	129.55	350.00	2.54	3.33
2BTR	19	261.344	0.10	-1.02	6.50
2BTS	24	300.417	0.02	-1.70	8.94
2C4G	22	270.294	1.15	0.06	13.18
2C5O	17	207.275	6.50	0.81	3.12
2CLX	21	218.221	3.50	0.54	6.94
2EXM	17	203.249	78.00	1.89	7.84
2R3H	19	239.282	20.00	1.30	4.18
2VTA	10	118.139	185.00	2.27	6.05
2VTH	18	223.249	120.00	2.08	1.97
2VTJ	22	286.739	1.90	0.28	1.68
2VTL	16	187.203	97.00	1.99	7.89
2VTM	11	144.137	1000.00	3.00	1.68
2VTN	22	262.246	0.85	-0.07	9.11
2VTR	16	234.67	1.50	0.18	5.34
3BHT	20	241.255	0.01	-1.96	6.28
3BHV	26	293.291	0.08	-1.10	7.30
3EJ1	20	252.281	0.12	-0.92	6.41
3FZ1	24	278.352	0.15	-0.84	0.12
3PXY	22	233.233	5.90	0.77	3.66
3QQK	21	259.328	15.00	1.18	7.87
3QTQ	21	262.332	3.10	0.49	6.67
3QTR	24	295.361	0.93	-0.03	10.90
3QTW	24	296.349	0.65	-0.19	11.51
3R8Z	21	262.332	49.00	1.69	6.57
3RZB	20	236.294	100.00	2.00	9.31
3TIY	20	220.185	17.00	1.23	3.38
3TIZ	23	265.314	150.00	2.18	2.23
4EZ3	25	296.305	45.00	1.65	2.33

Supplementary Table 6

List of ligands in the BRD4 test set. Ligands highlighted in red are not included in the correlation plotted in Supplementary Figure 5 and Supplementary Figure 26.

PDB	No.Atoms	MW	IC50 or Kd (nM)	Log IC50	W_{QB} (kcal/mol)
3MXF	31	458.00	49.00	-1.31	6.63
3U5J	22	308.77	2460.00	0.39	7.00
3U5L	23	323.78	640.00	-0.19	9.12
4A9L	22	325.38	30000.00	1.48	4.78
4C66	23	343.85	79400.00	1.90	3.92
4CFK	23	307.35	1830.00	0.26	3.13
4CFL	23	306.36	1330.00	0.12	3.63
4E96	24	347.39	136.00	-0.87	4.51
4HBV	13	241.09	23000.00	1.36	2.51
4HBW	18	269.32	4800.00	0.68	5.98
4HBX	20	295.36	1900.00	0.28	5.53
4HBY	22	317.36	4400.00	0.64	5.42
4HXR	21	338.41	4100.00	0.61	6.54
4HXS	23	346.42	4100.00	0.61	4.90
4J0R	22	295.34	386.00	-0.41	7.70
4J0S	22	295.34	382.00	-0.42	7.10
4LR6	13	174.20	33000.00	1.52	3.85
4LZS	15	208.26	16000.00	1.20	2.84
4MEN	20	267.33	125000.00	2.10	3.84
4MEO	22	292.34	250000.00	2.40	5.73
4MEQ	17	225.25	250000.00	2.40	4.62
4O72	30	413.49	1000.00	0.00	9.00
4O74	38	521.66	25.00	-1.60	1.67
4O77	25	331.35	2500.00	0.40	1.10
4O78	30	406.44	4600.00	0.66	4.07
4O7A	23	349.17	19000.00	1.28	3.72
4O7E	24	313.36	5700.00	0.76	0.00
4PCE	19	253.34	7000.00	0.85	4.30
4PCI	19	252.31	7500.00	0.88	4.84
4UYD	15	205.22	79400.00	1.90	4.03